Methods for Nitrogen Activation by Reduction and Oxidation

H. Iriawan[1,2,9], S.Z. Andersen[3,9], X. Zhang[4,5], B. M. Comer[6], J. Barrio[2], P. Chen[4†], A.J. Medford[6†], I.E.L. Stephens[2†], I. Chorkendorff[3†], Y. Shao-Horn[1,7,8†]

[1]Department of Materials Science & Engineering, Massachusetts Institute of Technology
[2]Department of Materials, Imperial College London
[3]Department of Physics, Technical University of Denmark
[4]Dalian National Laboratory for Clean Energy, Dalian Institute of Chemical Physics, Chinese Academy of Sciences
[5]University of Chinese Academy of Sciences, Beijing, 100049, China
[6]School of Chemical & Biomolecular Engineering, Georgia Institute of Technology
[7]Department of Mechanical Engineering, Massachusetts Institute of Technology
[8]Research Laboratory of Electronics, Massachusetts Institute of Technology

[9]These authors have contributed equally

[†]Corresponding authors

Abstract

The industrial Haber-Bosch process to produce ammonia (NH_3) from dinitrogen (N_2) is crucial for modern society. However, N_2 activation is inherently challenging and the Haber-Bosch process has significant drawbacks, as it is highly energy intensive, not sustainable due to substantial CO_2 emissions primarily from the generation of H_2 and requires large-centralized facilities. New strategies of sustainable N_2 activation, such as low-temperature thermochemical catalysis and (photo)electrocatalysis, have been pursued, but progress has been hindered by the lack of rigor and reproducibility in the collection and analysis of results. In this Primer, we provide a holistic step-by-step protocol, applicable to all nitrogen-transformation reactions, focused on verifying genuine N_2 activation by accounting for all contamination sources. We compare state-of-the-art results from different catalytic reactions following the protocol's framework, and discuss necessary reporting metrics and ways to interpret both experimental and density functional theory results. This Primer covers various common pitfalls in the field, best practices to improve reproducibility and cost-efficient methods to carry out rigorous experimentation. The future of nitrogen catalysis will require an increase in rigorous experimentation and standardization to prevent false positives from appearing in the literature, which can enable advancing towards practical technologies for the activation of N_2.

[H1] Introduction

[H2] Importance of NH_3 for Population Growth

Nitrogen is essential to all forms of life and constitutes ~78 % of air in the form of dinitrogen (N_2). However, the formidable strength of the N≡N triple bond (bond dissociation energy of 9.80 eV per bond at 298 K)[1] makes N_2 fixation into biologically-available forms extremely difficult[2]. N_2 fixation in nature occurs in two ways. Lightning can convert N_2 in air to nitrous oxides (NO_x)[3]. More dominantly, nitrogenase enzymes can catalyse N_2 reduction to ammonia (NH_3) by a multi-electron transfer process. The other process involves the hydrolysis of at least 16 equivalents of adenosine triphosphate (ATP) to produce 2 molecules of NH_3 and at least 1 molecule of dihydrogen (H_2), alongside adenosine diphosphate (ADP) and phosphate (P_i) release ($N_2 + 8\ H^+ + 8\ e^- + 16ATP \rightarrow 2\ NH_3 + H_2 + 16ADP + 16\ P_i$)[4]. This system performs at up to 65% selectivity to NH_3 at 1 atm N_2 in the absence of N_2O [REF[4,5]]. Yet, biological N_2 fixation is kinetically slow due to reliance on electron tunnelling[6] and is insufficient to sustain intensive modern agricultural practices[7].

Prior to industrial production of NH_3 by the Haber-Bosch process, natural fertilizers came in the form of caliche from Chile and guano from Peru[8]. In 1898, Sir William Crookes deemed mass starvation to be the biggest challenge of the 20th century[9], instigating the burgeoning interest in industrial N_2 activation. In 1903, the Birkeland-Eyde process became commercial[7], utilizing electric arcs to fix atmospheric N_2 into nitric acid (HNO_3), based on a method used by Henry Cavendish in 1784[10]. In 1908, Fritz Haber managed to synthesize NH_3 from N_2 and H_2 ($N_{2(g)} + 3H_{2(g)} \leftrightharpoons 2NH_{3(g)}$, ΔG° = -32.9 kJmol^{-1} (REF[11]), eq. 1) on a table-top machine, but it suffered from remarkably slow kinetics under standard temperature and pressure[8]. To boost the formation rate of NH_3 and tilt the equilibrium, Haber increased both temperature and pressure over an Os catalyst[7]. Subsequently, BASF bought the invention and Carl Bosch up-scaled the production in 1913[7] to the currently known Haber-Bosch process, which operates at 400-450 ^{o}C and 150-250 bar over a multi-promoted fused Fe catalyst[12]. This system can be referred to as Gen 1 (**Fig. 1**) and is currently the main commercially available process for NH_3 synthesis. A more active Ru-based supported catalyst was later developed, but it was not as widely adopted due to drawbacks such as high cost and low stability [13]. Gerhard Ertl elucidated the molecular mechanistic details of the catalytic N_2 reduction to NH_3 over Fe, enriching the understanding of the system[14], for which he was awarded a Nobel Prize in 2007 (**Fig. 1**).

Industrial NH_3 production by the Haber-Bosch process is the backbone of modern society and is responsible for the population boom in the 20th century[15–17]. Current annual NH_3 production exceeds 170 million metric tonnes[18] (Mt) globally, of which ~80 % is used as synthetic fertilizer[19], thereby providing sustenance for two-fifths of the global population[20]. Moreover, NH_3 is the source of every N atom in all synthetic chemicals[21], a key reactant in the chemical industry[22] and a potential hydrogen energy carrier[23,24]. However, NH_3 production from the Haber-Bosch process is energy and emission intensive. Nearly all the required energy and emissions in NH_3 production originate from the generation of H_2, most commonly from natural gas via steam-methane reforming[25] ($0.75CH_{4(g)} + 1.5H_2O_{(l)} \leftrightharpoons 3H_{2(g)} + 0.75CO_{2(g)}$, ΔG° = +98.0 kJmol^{-1} (REF[11]), eq. 2). For the methane-fed process, NH_3 production has a theoretical minimum energy input of 22.2 GJt_{NH3}^{-1} with the stoichiometric emission of 1.2 $t_{CO2}t_{NH3}^{-1}$ (REF[12]). In comparison, modern NH_3 production plants using the best available technology consume 28-33 GJt_{NH3}^{-1} and emit 1.6 $t_{CO2}t_{NH3}^{-1}$ (REF[12,25]), but the global average is 2.9 $t_{CO2}t_{NH3}^{-1}$ (REF[26]) owing to the use of coal and oil-based feedstocks[12]. The annual global NH_3 production (>170 Mt) consumes about 1% of total world energy production and emits 1.4% of global CO_2 emissions[18,25,27]. Implementation of CO_2 sequestration processes

or other carbon offsets can reduce emissions but will add cost, plant complexity and energy losses[28]. Overall, sustainable alternatives for NH_3 production are required to address climate change challenges by reducing reliance on fossil fuels.

[H2] Decarbonization of N_2 activation

Replacing the generation of H_2 by steam-methane reforming with renewable water splitting ($3H_2O_{(l)} \leftrightharpoons 3H_{2(g)} + 1.5\ O_{2(g)}$, $\Delta G^\circ = +711.4$ kJmol^{-1} (REF[11]), eq. 3) can eliminate CO_2 emissions associated with the Haber-Bosch process[12], referred to as Gen 2 (**Fig. 1**), resulting in an energy expenditure of $\Delta G^\circ = +678.5$ kJmol^{-1} (REF[11]) for $N_{2(g)} + 3H_2O_{(l)} \leftrightharpoons 2NH_{3(g)} + 1.5\ O_{2(g)}$ (eq. 4). Operating the Haber-Bosch at reduced temperatures and pressures and coupling with renewable H_2 production via water electrolysis could make NH_3 production sustainable and reduce capital cost via smaller, local reactors. However, major challenges need to be addressed[29], including: synthesizing NH_3 at milder conditions (pressures of 20-40 bar) to cope with the intermittent and low-pressure influent of H_2 from water electrolysis; sustainable separation of pure N_2 from air, as N_2 is presently separated from O_2 by combustion of unreacted methane; and the discovery of low-temperature thermochemical catalysts to achieve high yield per pass at moderate pressures.

Electrochemical reduction of N_2 and H_2O to make NH_3 is an attractive strategy because NH_3 can be synthesized directly at the point of consumption, eliminating transportation cost and emissions and reducing issues of excess fertilizer run-off[30,31]. The energy expenditure of $\Delta G^\circ = +678.5$ kJmol$_{\text{fixed N2}}^{-1}$ (eq. 4) or 19.9 GJt$_{NH3}^{-1}$ for such process can be provided by using (photo)electrochemical systems powered by solar or wind (Gen 3, see **Fig. 1**). Assuming 5% electrical-to-NH_3 efficiency (the calculation neglects upstream and downstream separations, see Supplementary Information for details), 40 m^2 of state-of-the-art solar cells operating at 20% efficiency should meet the average nutrient requirement of 100 kg of fixed N (expressed as monatomic nitrogen) per hectare of land per year, making this process sustainable and economical.[32,33]. The current densities will need to be comparable to those of the state-of-the-art electrolysers to keep down capital costs; the US Department of Energy has a target[34] of 300 mA cm$^{-2}_{geo}$ at 90% Faradaic efficiency **[G]**.

The reduction of N_2 can also be facilitated by non-thermal plasmas, where vibrational excitations of ground-state N_2 via collision with high-energy electrons can decrease the N_2 activation barriers **[G]**[35]. Typically, microwave and dielectric barrier discharge **[G]** (DBD) reactors have been used, where the NH_3 synthesis rate can be increased through heterogeneous catalysis[36]. Kim *et al.* have reported among the highest energy efficiencies of 25-35 g_{NH3} kWh^{-1} (100-140 GJ t_{NH3}^{-1}) using a DBD reactor and promoted Ru catalyst[37], but the challenges lie in the uncompetitive energy efficiency compared to commercial Haber Bosch (28-33 GJ t_{NH3}^{-1}) and NH_3 decomposition[38]. Additionally, recent reports suggest a mechanocatalytic method of NH_3 synthesis under (near) ambient conditions[39,40], by ball-milling the catalysts under N_2 and subsequently introducing H_2, showing early promise of comparable energy efficiency to the Haber-Bosch[39].

Electrochemical oxidation of N_2 by electrolysis to fixate N_2 ($N_{2(g)} + H_2O_{(l)} + 2.5O_{2(g)} \leftrightharpoons 2HNO_{3(aq)}$, $\Delta G^\circ = +14.6$ kJmol^{-1}, eq. 5) expends much less energy than $\Delta G^\circ = +678.5$ kJmol^{-1} (REF[11]) for the reductive counterpart (eq. 4). Such process can in principle replace the synthesis of NH_3 and subsequent oxidation of NH_3 by the Ostwald Process ($2NH_{3(g)} + 4O_{2(g)} \leftrightharpoons 2HNO_{3(aq)} + 2H_2O_{(l)}$; $\Delta G^\circ = -663.9$ kJmol^{-1} (REF[11], eq. 6) for the production of nitric acid (aqueous HNO_3 is fully ionized), a primary commodity chemical of oxidized N_2[41]. The remarkable difference in the energy expenditure for N_2 fixation between reduction and oxidation can be noted clearly by standard potentials **[G]**of electrochemical half-cell reactions **[G]** plotted

on the standard hydrogen electrode (SHE) scale and also on the absolute electron energy scale referenced to the free electron in vacuum[42], as shown in **Fig. 2a**. The standard potential for N_2 reduction ($N_{2(g)} + 6H^+ + 6e^- \rightarrow 2NH_{3(g)}$, 0.06 V_{SHE}, -4.50 eV) is considerably higher than that of water splitting to generate O_2 ($2H_2O_{(l)} \rightarrow O_{2(g)} + 4H^+_{(aq)} + 4e^-$, 1.23 V_{SHE}, -5.67 eV). The difference indicates the energy need of pumping electron energy from -5.67 eV to -4.50 eV for each electron transferred, in agreement with standard reaction free energy of +678.5 kJmol^{-1} for $N_{2(g)} + 3H_2O_{(l)} \leftrightharpoons 2NH_{3(g)} + 1.5O_{2(g)}$ (with 6 electrons transferred from the cathodic to anodic half reactions). On the other hand, the standard potential for N_2 oxidation ($N_{2(g)} + 6H_2O_{(l)} \rightarrow 2NO_3^-{}_{(aq)} + 12H^+_{(aq)} + 10e^-$, 1.24 V_{SHE}, -5.68 eV) is very similar to that of water splitting to generate O_2 ($2H_2O \rightarrow O_{2(g)} + 4H^+ + 4e^-$, 1.23 V_{SHE}, -5.67 eV), where minimum energy is required to activate N_2 and H_2O to make NO_3^- from the thermodynamic standpoint.

Since N_2 activation is the challenging step, once N_2 is activated, N-containing compounds can easily be converted to other N-containing compounds. To this end, direct conversion to nitric oxide (NO) from N_2 and O_2 via plasma driven processes[43] does not require NH_3 synthesis as an included step. The most technologically mature form of N_2 oxidation is the Birkeland-Eyde process, which is assisted by electric arc-generated hot plasma**[G]**[44,45]. High-temperature thermal plasmas are not energy-competitive[46] and require rapid quenching to prevent NO decomposing back to N_2[47]. Researchers are paying increasing attention to the use of warm and cold (non-thermal) plasmas, as its theoretical energy consumption[48] is more than two-fold lower than that from N_2 and CH_4, yet a technological bottleneck lies in low conversion to product[49]. More recently, a growing number of studies are dedicated to the electron and photon assisted conversion of N_2 to nitrate (NO_3^-)[50–56] but seem to suffer significant kinetic limitations similar to the reductive counterpart.

[H2] Origin to N_2 activation challenges

Activating N_2 by reduction to make NH_3 is kinetically difficult, which demands much more energy than what is needed thermodynamically to drive reactions at high rates to make these processes economical. Catalyzing N_2 fixation has been limited largely by the cleavage of the N≡N bond due to the inertness of N_2 (REF[2]), as related to the high triple bond strength (9.80 eV), high ionization potential (15.84 eV), low electron affinity (−1.90 eV) and nonpolarity. Ru is considered the most active elemental heterogenous catalyst for thermochemical NH_3 synthesis (the Haber-Bosch process). The energetics of the possible elementary steps are examined. The free energy profile for an associative mechanism on Ru(0001) terrace, which involves N_2 bond cleavage via a hydrogenated intermediate (similar to nitrogenase[6]), is shown in **Fig. 2a**. The protonation of adsorbed $*N_2$ to $*N_2H$ (step 1-2, where * denotes adsorbed species) has the largest thermodynamic barrier, i.e. the largest energy difference between sequential states, of 1.1 eV compared to the other elementary steps. This $*N_2$ protonation step to $*N_2H$ is considered rate-limiting by invoking the Brønsted–Evans–Polanyi relationship[57], which linearly correlates the activation barriers to the reaction energies. In contrast, Ru(0001) step sites adsorb N_2 more strongly than terrace sites and the thermodynamic barrier at the step sites for $*N_2$ to $*N_2H$ is much lower (~0.35 eV) as a result of stronger adsorption on a more undercoordinated site. In addition, the process can be understood commonly via a dissociative mechanism[58–60], where N_2 is cleaved upon adsorption into atomic N, and then hydrogenated to release NH_3. Although the dissociation of N_2 to 2*N is thermodynamically favored, this step has a significant activation barrier, and occurs only at step sites as a result of the prohibitively high activation barrier for N_2 dissociation on terrace sites[61,62]. Experimentally, the apparent activation barrier on a clean Ru(0001) single crystal (containing step site density of ~1%) is 0.4 eV and increases to 1.3 eV when small

amounts of Au, which preferentially decorate step sites, is introduced, which demonstrates that the rate of N_2 dissociation is completely dominated by steps[62]. It is worth noting that an activation energy found from the Arrhenius plot corresponds to the potential energy barrier that only captures the enthalpy term. Thus, to evaluate the free energy of activation (displayed in **Fig. 2a**), the energy associated with the loss of gas phase entropy of N_2 as it is bound on the surface has to be included (see Creating free energy diagrams under Results for further details). Moreover, there are also significant uphill steps for the reduction of $*NH_2$ to $NH_{3(g)}$ (step 6-8) at the step sites on Ru(0001), signifying the cost of creating free sites. The apparent activation energy is the sum of both the activation energy of the rate-limiting step and the cost of making free sites in a non-trivial manner[61,63]; this is the origin of the Sabatier principle.

Activating N_2 by oxidation is equally challenging, and very few systematic investigations on the oxidative N_2 fixation have been reported in the literature[67,68]. A reasonable starting point would be to consider a series of hydroxylation-deprotonation steps as computed for N_2 oxidation on rutile RuO_2 (110)[56] in **Fig. 2a**, which shows N_2 activation to $*N_2OH$ is the most uphill step (1.9 eV), suggesting a large kinetic barrier.

An important distinction between electrochemical and non-electrochemical steps should be made when interpreting free energy diagrams. Electrochemical steps, such as those involving proton-electron transfers (see all steps in **Fig. 2a** except for N-N dissociation, adsorption and desorption), are affected by applied potential. The overpotential required to bring the most uphill electrochemical step downhill is plotted in **Fig. 2b** (blue, circle) for associative N_2 reduction on transition metal terraces. In addition to the thermodynamic barrier, electrochemical steps can possess an additional kinetic barrier. For example, the intrinsic electrochemical barrier (at $\Delta G_{step} = 0$) for the $*N + e^- + H^+ \rightarrow *NH$ step on transition metal terraces were calculated as ~0.7 eV regardless of the free energy difference between the two states (*N and *NH), and thus insensitive to the metal identity[66]. An intrinsic barrier of 0.7 eV for all proton-electron transfer steps is used in **Fig. 2a**. Non-electrochemical steps, such as N-N dissociation (step 0-1 of the dissociative N_2 reduction, **Fig. 2a**), adsorption (step 0-1 of the associative N_2 reduction/oxidation) and desorption (step 7-8 of N_2 reduction), are not affected by applied potential.

The rate-limiting step, known as the maximum barrier along the reaction pathway whose rate is significantly slower than those of the other elementary steps, is a feature of interest as it governs the rate of the overall reaction. The rate constant (k) of the elementary step is given by **eq. 7** from transition state theory

$$k = \nu \, exp(\frac{-\Delta G^{\ddagger}}{k_B T}) \qquad \text{(eq 7.)}$$

where the prefactor ν equals k_BT/h (~10^{13} s^{-1} at 25 °C). The rate of reaction for heterogenous catalysis, expressed in mol cm_{cat}^{-2} s^{-1}, is connected to the rate constant by multiplying that with the concentrations of reactants or with their surface concentrations if the rate limiting step is the first step or involves surface intermediates, respectively. This rate can be converted to the turnover frequency (mol $site^{-1}$ s^{-1}) by dividing the site area density of the catalyst (sites cm^{-2}_{cat}), to mass activity (mol g_{cat}^{-1} s^{-1}) by multiplying the specific surface area (cm_{cat}^2 g_{cat}^{-1}), and to geometric-area-normalized activity (mol cm_{geo}^{-2} s^{-1}) by multiplying the roughness factor (cm_{cat}^2 cm^{-2}_{geo}).

To rationalize a catalyst's viability, one can calculate the rate constant to estimate the rate and establish the point at which the barrier on a catalyst becomes prohibitive, which will be defined below. In using eq. 7, we note that the errors due to the level of theory and a free energy correction of ~0.25 eV[67,68] correspond to ~5 orders of magnitude difference in rate. Generally, an active catalyst would have a turnover frequency

[G] greater than 1 s^{-1}, which corresponds to a barrier of ~0.75 eV at room temperature. Therefore, free energy diagrams for electrochemical N_2 fixation under ambient conditions that involve an uphill step greater than 1.5 eV at the operating potential indicate non-viable catalysts, particularly if kinetic barriers have been neglected. However, a more quantitative and accurate description requires higher forms of simulation to capture the system's complexity, such as kinetic Monte Carlo simulation or microkinetic modelling; the latter shown in **Fig. 2b** for the thermochemical route of NH_3 synthesis. For the electrochemical route, we refer readers to REF[66] for the full microkinetic model **[G]**.

The difficulty of finding catalysts with fast kinetics for N_2 fixation can be explained by the "scaling relations"[69], where the energetics of different elementary steps (**Fig. 2a**) cannot be controlled independently on a given surface. Such scaling relations can be manifested in the volcano dependence of catalytic activity on the adsorption energy of surface reaction intermediates. For example, the catalyst activity, computed via the mean-field kinetic model **[G]** of the dissociative mechanism, exhibits a volcano dependence on the N adsorption energy (**Fig. 2b,** circle, red)[69]. On the right side of the volcano N_2 dissociation is rate-limiting for weak-binding surfaces, and on the left side there is a low barrier for N_2 dissociation for strong-binding surfaces, but the surface is poisoned by N species. Fe, Ru and CoMo alloy exhibit the highest activity and further enhancement can be achieved by using alkali (electronic) promoters[70,71]. However, efficient and low-pressure Haber Bosch requires more active catalysts beyond the constraints set by the volcano[72].

Scaling relations also constrain electrochemical N_2 reduction. The overpotential needed to have all the elementary reaction steps downhill for the associative mechanism (**Fig. 2b**, circle, blue), exhibit a volcano relationship with the N binding energy on metal surfaces[73,74]. More importantly, electrochemical N_2 reduction in aqueous electrolytes has to compete with electrochemical H_2 evolution as both reactions have similar standard potentials and electron energy on the absolute energy scale (**Fig.2a**). This competition is a disadvantage, as the kinetics of water reduction to produce H_2 is much faster than that reduction of N_2 to NH_3, as seen in the comparatively lower overpotential for H_2 evolution (**Fig. 2b**, blue, triangle), translating to many orders of magnitude difference in the estimated rate (**Fig. 2b**). In addition, the bond strength of any given metal surface to H (a sole intermediate of H_2 evolution) is stronger and linearly correlates with N-containing intermediates of N_2 reduction[32], which indicates that the surface will be poisoned by *H[75] and is likely responsible for negligible NH_3 reported in aqueous systems[76,77]. Although a study on wider N_2 electrooxidation trends has yet to be reported, a similar scaling relation between the reactant activation and subsequent hydroxylation or desorption steps is expected, as well as scaling with $*O_2$ intermediates of the competing O_2 evolution.

Alternative strategies have been explored to overcome the activity and selectivity challenges in N_2 reduction. Excellent activities using transition metal-LiH composite catalysts in thermochemical NH_3 catalysis have been reported. In these systems, two active centers are present; transition metal sites to cleave the N_2 bond, and LiH to aid N hydrogenation and subsequent NH_3 desorption[78]. In electrochemical NH_3 synthesis, the lithium-mediated approach has emerged, where the N_2 reacts with metallic Li to form Li_3N, followed by nitride protonation to evolve NH_3, including continuous lithium-mediated N_2 reduction in non-aqueous solvents[79–82] or a lithium-nitride cycling scheme[83,84] (**Fig. S2**, see Supplementary Information). The Li-mediated approach has decoupled reactant activation and subsequent protonation steps, while the non-aqueous solvent and the in-situ formation of protective solid-electrolyte-interphase layer restrict proton availability to the active site[82,83], potentially responsible for the high yields.

[H2] The need for a strict protocol

Progress in (photo)electrochemical N_2 fixation can benefit from developing a more rigorous protocol of measurements and product quantification, as state-of-the-art yields of NH_3 (and NO_3^-) from these processes are significantly lower than thermochemical NH_3 production (see Results) while contamination (possible sources summarized in **Table 1**) can be present at similar or greater concentration levels than the measured product[76]. In addition, the NH_3 yields for low-temperature and/or low-pressure thermal catalysis exponentially drops, and accurate activity measurements can suffer from adventitious N contamination, N and/or H leaching and non-catalytic NH_3 generation[85], where such uncertainties in catalytic activity measurements can propagate into subsequent kinetic analyses.

The field has been plagued with false positives. The first observation of electrochemical N_2 fixation was in 1807 reporting production of NH_3 and HNO_3 by passing current through distilled water[86], but was proven non-reproducible some 90 years later[87]. In 1995, the inability to reproduce reported photochemical NH_3 synthesis using TiO_2 under rigorous measurements was rigorously reported[88]. More recently, Sn(II) phthalocyanine catalysts were tested in 2017 for electrochemical N_2 reduction, concluding that the NH_3 initially measured arose from decomposition of the catalyst[89]. Work on nanoscale Fe_2O_3 in molten hydroxide citing adventitious NH_3 synthesis from trace NO_x^- contaminants in their electrode material was later retracted from *Science* in 2020[90]. Others have retested and reported no electrochemical activity for VN[91], and Bi and Au catalysts[92], reported previously to have high activity[93–95], after accounting for N-leaching from the VN catalyst and properly cleaning the supplied N_2 gas for NH_3 and NO_x impurities.

The ubiquity of contamination sources calls for an exceptional scrutiny. In this Primer, we introduce a general protocol focused on confirming genuine activation of inert N_2 and elaborate details in performing catalytic measurements (Experimentation). We then evaluate state-of-the-art results, primarily focused on (photo)electrochemical and thermochemical systems using the protocol's framework, and discuss best practices in reporting and interpreting both experimental and density functional theory **[G]** (DFT) data (Results). The potential uses of these N_2 activation reactions are discussed in the context of current practices, highlighting the importance of research in these areas (Applications), and we explore factors affecting reproducibility, thereby establishing reporting standards (Reproducibility and Data Deposition). Finally, we discuss ways to overcome cost-limitations of performing repeated isotope-labelled experiments (Limitations and Optimizations), and outline future directions in N_2 activation research including community-wide adoption of rigorous protocol, in situ measurements for mechanistic understanding and field-specific needs (Outlook).

[H1] Experimentation

A general protocol for carrying out electrochemical, photo(electro)chemical, and thermochemical N_2 activation experiments is presented, which can be applied across all N_2 activation fields. The unified protocol is followed by an in-depth discussion of the experimental setups and necessary measurements, and different methods of product detection to determine product synthesis.

[H2] Protocol for N_2 reduction and oxidation

The general protocol highlighted in **Fig. 3** is applicable to any N_2 activation reaction and is based on the principle that one should always be wary of contamination, which should be accounted for accordingly.

The first step involves the experiment setup and is run with N_2. If no product is measured, re-iterations with new parameters or catalysts is necessary, until the desired product is detected. To account for possible contamination sources, one must measure or estimate the total equivalent N mass of the system, $mass_{sys}$, which includes $mass_{N,cat}$, $mass_{N,electrolyte}$, $mass_{N,absorber}$ and $mass_{N,gas}$. Precise definitions of these terms are outlined in **Box 1**.

The amount of N in the product measured must exceed the amount of N in $mass_{sys}$ by a factor of 2 ($mass_{prod}$ > 2 $mass_{sys}$) – to account for unexpected sources of contamination– and $mass_{prod}$ should be well above $mass_{N,cat}$ for synthesis to be classified as effective. The product concentration (C_{prod}) in the electrolyte or gas stream must be higher than 100 ppm, as this amount would easily be detectable by olfaction as per the NH_3 detection limit[96] and greater than a common source of contamination in the lab, in which case unaccounted sources of contamination (for example, glassware, breath, laboratory air, etc.) could be excluded.

If both criteria are met, repeated testing is necessary with independently prepared samples to confirm reproducibility. If these criteria were not met, the measured yield of product might stem from contamination, and further evidence of product synthesis via quantifiable isotope-labelling experiments is necessary. First, one must test using an inert gas (such as Ar, although any clean inert gas can be used) and test N_2 in the absence of a driving force. These conditions can range from operating an open circuit potential for electrochemical systems, analysis under dark illumination for photo(electro)chemical systems or in the absence of applied heat for thermochemical systems. Operating under these driving force-free conditions is essential to account for sources of contamination in the experimental set-up, as this should give significantly less to no product compared to N_2 with a driving force. Repeated identical testing of independently prepared batches also follows to ascertain reproducibility and determine the level of inherent contamination (if any) in the system. A stability test is also needed to eliminate the possibility of non-catalytic generation of the product, such as N-leaching from an N-containing catalyst. Once all sources of contamination have been accounted for, quantitative isotopic labelling experiments is necessary. Two separate quantification techniques must be used to detect the product, where at least one of these methods is isotopically sensitive, and repeated and reproducible overlap between the use of $^{14}N_2$ and $^{15}N_2$ over multiple points must be observed (see Results). It is important to include a proper gas cleaning procedure, as isotope labelled $^{15}N_2$ gas can contain significant levels of NO_x and NH_3 impurities[97].

Kinetics parameters, such as activation energy and reaction orders **[G]** in the kinetic regime, are a key metric to report when studying thermochemical catalysis. The kinetics measurements should be carried out far from the equilibrium, where mass and heat transfer limitations are minimized, to avoid the reaction reversing. Measurements that enable extracting the activation energy and reaction orders are extremely beneficial for elucidating the reaction mechanism. In particular, the effect of NH_3 concentration on the reaction orders and the apparent activation energy must be accounted for (see Results). Electrochemical and photo(electro)chemical systems can also benefit from kinetic measurements, although this is not common in the literature. To this end, reliable determination of the partial current density toward NH_3 for a given system might be highly inaccurate owing to historic contamination issues in the field, which makes obtaining these measurements difficult. Measuring parameters such as the pH dependence of the N_2 reduction activity might provide insights on the reaction path and mechanism[98] using rigorous

experimentation. The only published and proven work reporting kinetic measurements have investigated the effect of proton and N_2 concentration and their respective reaction orders in the lithium-mediated system[81]. Tafel analysis **[G]** can be a powerful tool for elucidating rate determining steps, but overly simplified assumptions will lead to an inaccurate description of the electrocatalysis[99], so researchers should apply caution when interpreting Tafel slopes as they may contain many artefacts[100]. Overall, great care should be taken with reporting a clear definition of the kinetic parameters and kinetic models used[101] when including these sets of measurements.

[H2] Experimental setup

[H3] Electrochemical measurements

Electrochemical measurements are typically conducted in a cell setup as depicted in **Fig. 4a**, into which gas streams are introduced. Feed gases (Ar, $^{14}N_2$, and $^{15}N_2$) must be cleaned prior to use as they can contain significant amounts of activated N-species (such as NH_3, NO_x and N_2O) as contaminants[97,102]. This purifying process involves using a reduced Cu catalyst and freeze trap[76] or commercial gas purifiers. One can also choose to not clean the gas and measure all the N-containing contaminants to include in the value for $mass_{N,gas}$. In the electrochemical cell, the working electrode (WE) will either facilitate N_2 reduction or oxidation, while the counter electrode (CE) runs the respective counter reaction, depending on the reaction being evaluated. Meanwhile, the reference electrode (RE) determines the potential at the surface of both other electrodes. In aqueous electrolytes, numerous commercial REs are available[103] and should be calibrated against the reversible hydrogen electrode (RHE) by measuring the equilibrium potential for H_2 oxidation and its evolution on a Pt electrode. Alternatively, a well-known RE such as saturated calomel electrode (SCE) in aqueous electrolytes, or Li in non-aqueous electrolytes can be utilized, with a conversion to RHE. Calibrating the RHE in non-aqueous electrolytes can be challenging[104], but is possible because the H_2 oxidation and evolution potential is measurable for lithium-mediated N_2 reduction[80]. The same REs as those used in the battery literature can be used when measuring N_2 reduction in non-aqueous electrolytes, such as metallic Li[105], and calibrate the RE to the RHE scale in their electrolyte of choice in a separate measurement.

As activated N-species are ubiquitous, electrochemical and photo(electro)chemical systems are prone to contamination. Possible sources of contamination are shown in **Table 1**, along with a recommended method of elimination. Specifically, the commonly used Nafion membrane has been shown to contaminate the setup[76,106,107] and degrade in the presence of NH_3[108,109], so extra care must be taken if using this membrane. For a porous membrane like Celgard, an NH_3 crossover between electrode compartments has been observed under applied potential condition[77], which may lead to irreproducible yields especially during a long-term evaluation. Caution must be taken when using a downstream acid trap in collecting the residual NH_3 from the gas stream as an acidic solution can readily absorb NH_3 from the environment. Overall, the extent to which all of these factors influence product quantification must be assessed when reporting catalyst performance.

Control experiments, such as testing using Ar with a driving force and N_2 without a driving force with time-dependent experiments, are needed. All adventitious sources of activated N_2 can be avoided by the use of purified isotopically labelled $^{15}N_2$, and the subsequent measurement of $^{15}NH_3$ or $^{15}NO_x$ by an isotope sensitive method[76,77]. Liquid samples from the electrolyte should be investigated, repeated for reproducibility and quantified via at least two separate methods, and the yield produced using $^{15}N_2$ must be comparable to the yield measured with $^{14}N_2$.

Chronopotentiometric (CP) and/or chronoamperometric (CA) measurements show the stability of the system over time, and representative data for these should be reported, with a description of whether Ohmic correction **[G]** is utilized. When probing the potential across the electrochemical interface in question, an iR-correction, based on the pre- or post-testing ohmic drop, is generally encouraged as it can eliminate the system-dependent effects, such as electrolyte conductivity and electrode geometry. However, such correction must be done with caution especially if the ohmic drop varies during testing owing to factors such as bubble formation, rising electrolyte levels, temperature variation, build-up of non-conducting phases observed in the Li-mediated process, among others. In such cases, the potential should be reported as a range of values rather than a single point. Once the synthesized product is detected, the product yield and Faradaic efficiency can be calculated as a function of potential *vs* RHE, enabling the determination of the optimum for each of these factors in the system. Moreover, the difference between the operating potential and the equilibrium voltage approximates the overpotential, a critical figure-of-merit. The overpotential for N_2 reduction to $NH_{3(g)}$ is independent of pH and the electrolyte. The Nernstian shift in the equilibrium potential occurs due to a change in product and reagent concentrations that affect the overall pH of the solution, and can be taken into account via the actual amount of NH_3 produced. Relative to standard conditions, the equilibrium concentration of $NH_{3(aq)}$ or $NH_4^+{}_{(aq)}$ can be determined by thermodynamic data (solvation energy) or measured directly via NMR[110]. At pH = 0, the difference between the standard equilibrium potential $N_{2(g)}/NH_4^+{}_{(aq)}$ is 0.27 V vs RHE, though at pH = 14, the standard equilibrium potential of $N_{2(g)}/NH_{3(aq)}$ is ~0.1 V vs RHE[11]. However, this Nernstian shift is insignificant when there is a large overpotential for N_2 reduction, such as the case for non-aqueous lithium-mediated NH_3 synthesis.

[H3] Thermochemical measurements

Thermochemical measurements are usually conducted in a fixed-bed flow system as shown in **Fig. 4b**, where the catalyst is loaded into the reactor and pretreated under specified conditions. The reactant gases (N_2 and H_2) are passed over the catalyst bed with a certain space velocity, such that the reaction rates are not limited by gas transport. The reactant gases may need purification by in-line gas purifiers to reduce the content of impurities (for example, H_2O, O_2, CO_2) to sub-ppm level, as these might affect the surface of the active catalyst by poisoning the available active sites. The measurements should be conducted under steady-state conditions as a function of temperature and pressure. The produced NH_3 is typically trapped in a downstream diluted sulfuric acid solution, which is then quantified by using ion chromatography or a conductivity meter. The related parameters (such as NH_3 synthesis rate and yield) can be obtained once the amount of produced NH_3 is determined.

Reactors made of stainless steel are commonly employed for pressurized reactions. Transition metals (including Fe, Cr, Ni) in the reactor may not be inert, and could interfere in the NH_3 synthesis by interacting with the catalyst. It is recommended to use a reactor made of, or lined with, inert material such as quartz to exclude the contribution of a "reactive reactor"[111]. A blank test (without catalyst loading) should be performed prior to catalyst evaluation, to make sure there is no detectable NH_3 contamination present in the system. In addition, benchmark catalysts, such as Cs-promoted Ru/MgO should be prepared and tested, with an activity comparable to that previously reported (Cs−Ru/MgO with 3–6 wt.% Ru loading should have an NH_3 formation rate from 8–14 mmol g_{cat}^{-1} h^{-1} at 400 °C and 10 bar)[112–114]. These two experiments are important for validating the testing system.

[H2] Product detection and Isotope Labelling

[H3] Non-isotopic product detection

UV-Vis spectroscopy allows the fast and easy quantification of NH_3 through the colorimetric reactions of either indophenol blue or Nessler's reagents, with a detection limit down to 10 ppb (~0.5 µM) NH_3 (**Fig. 5 a, b**). The method induces a chemical reaction between NH_3 and the reagents of choice, leading to the formation of a colorful dye that is quantifiable via UV-vis spectroscopy with a peak value at 640 nm for indophenol blue and 425 nm for Nessler's reagents[115]. Despite the simplicity of these techniques, interferences in the chemical reaction forming the colorful dye may be caused by the presence of different ions in the media (Fe^{3+}, Co^{2+} to S^{2-}, etc.), the reaction time and diverse pH conditions, which may impede accurate quantification of NH_3[116]. Nevertheless, some of these can be overcome by using Seignette reagent (also known as Rochelle salt), which allows the analysis of samples with high salinity[117]. Similar in principle to indophenol-based detection, the salicylate method is also commonly used to detect NH_3. Recently, a convenient methodology to correct the effect of strong Fe^{3+} interference by using an interference model requiring only three experimental curves was reported[118].

The Griess assay is widely adopted for the quantification of NO_2^-. To quantify NO_3^-, the sample can be reduced to NO_2^- using Zn powder[119]. However, this method should be used with caution as it suffers from a comparatively high limit of detection of 500 ppb (~10 µM) and interferences with Fe^{3+}, Cu^{2+}, S^{2-} or I^-.

A conductivity meter provides a facile and widely adapted method in thermochemical reactions for quantifying NH_3 with a 1 ppm detection limit (**Fig. 5a, c**). The concentration of NH_3 from the outlet gas trapped in a diluted sulfuric acid solution can be determined by measuring the decrease in ion conductivity of the solution, which corresponds to the conversion of H^+ to NH_4^+. A calibration curve of the change of conductivity and the amount of NH_3 produced should be determined under a given temperature and concentration of the solution. It is important to maintain a constant temperature and concentration of the solution in each measurement as each of these parameters have strong influences on the ion conductivity in the solution[120].

[H3] Isotopic Product detection

Nuclear Magnetic Resonance (NMR) is one of the most widely used techniques for determining the chemical composition of a sample, and can accurately detect NH_3 down to 50 ppb (~3 µM), as shown in **Fig. 5a, d**. It utilizes the magnetic properties of nuclei with non-zero spins and non-zero magnetic dipole moments. The sample composition can be determined based on the characteristic radio frequency (RF) pulse required for the excitation of the nuclei[121]. As the area of the signal is proportional to the number of nuclei affected by the applied RF pulse, the concentration of the sample can be inferred based on calibration curves. ^1H NMR can be used to differentiate isotopes of $^{14}NH_3$ and $^{15}NH_3$. Due to the difference in spin between ^{14}N and ^{15}N, the scalar interaction of ^1H will lead to respectively a triplet peak with a characteristic spacing of 52 Hz, and a doublet peak with a splitting of 73 Hz. For non-aqueous systems, the use of organic solvents might interfere with the detection of the NH_3 signal, however, different methods for solvent signal suppression have been reported[76,122].

In principle, the quantification of $^{14}NO_3^-$ and $^{15}NO_3^-$ can be performed using N-NMR. However, the low production yield of the experiment coupled with the unfavorable NMR properties of ^{15}N (low gyromagnetic ratio and long T1 relaxation constants)[123], implies that long-duration electrochemical experiments must be performed to allow reproducible quantification at multiple points. One study covering N_2 oxidation has used ^{15}N-NMR[56], but required >100 ppm concentration of NO_3^- for detection, which was achieved via a 50

hour experiment. Finding a more convenient isotopic NO_3^- detection method is a gap that must be addressed to enable measuring advances in electrochemical N_2 oxidation more easily.

[H1] Results

A state-of-the-art overview of electrochemical, photo(electro)chemical and thermochemical N_2 activation applying the protocol from the Experimentation section to determine levels of contamination is described. Important reporting metrics and issues hindering progress in the field is covered in this section, along with interpretation of both experimental and density functional theory results.

[H2] Evaluation of N_2 Catalysis Experiments

Product yields ($mass_{prod}$), namely NH_3 for N_2 reduction and NO_3^- for N_2 oxidation, relative to the size of the system from which N-contaminants may originate ($mass_{sys}$) are shown in **Fig. 6a**. Thermochemical systems typically produce several orders of magnitude more NH_3 (especially at temperatures >300 ºC) compared to $mass_{sys}$. As a result, these systems can cross the $mass_{prod} > 2\ mass_{sys}$ line within the first few hours of experimentation, and have experimental durations upwards to 100 hours (see Supplementary Information for a demonstration). The ease with which product yields in thermochemical experiments surpass the size of the system ($mass_{prod} >> 2\ mass_{sys}$) supports why contamination issues are not prevalent in thermal catalysis, and also inherently points towards an intrinsically high catalyst activity.

In contrast, electrochemical, photochemical and photoelectrochemical experiments typically show yields of NH_3 or NO_3^- in orders of magnitude less than the size of the system ($mass_{prod} << 2\ mass_{sys}$). None of these catalytic systems fulfill the $mass_{prod} > 2\ mass_{sys}$, and would require several orders of magnitude longer experimentation times (with proper gas cleaning) to afford more product. To this end, some suspiciously high yield rates from recent (photo)electrochemical studies have been reported (**Fig. 6b**), including the Bi point[95] operating at only -0.7 V_{RHE}, which reported production rates higher than some very active thermochemical catalysts operating at elevated pressure and temperature conditions. These results should have raised some concerns due to the reported high computed barrier (>2 eV) and the selectivity challenge against H_2 evolution[32] (see **Fig. 2b**). As the flagged point has been shown as non-reproducible[92], this example serves to highlight how adventitious N sources can lead to non-genuine N_2 fixation and inflate the reported yield rates. Comparison of the reported intrinsic activity (turnover frequency) with thermochemical catalysts also shows this conclusion (see **Fig. S3** in Supplementary Information) and can be used to screen potential false positives. In most cases, the catalytic activity of electro/photocatalysts are much lower than the thermal counterpart and so hundreds of hours of experimentation are required to surpass $mass_{sys}$ (see Supplementary Information for demonstration). Therefore, quantitative isotope-labelling experiments, along with a proper gas-cleaning protocol, is a convenient and unambiguous way to verify genuine N_2 fixation, thereby proving the origin of the activated N.

Non-aqueous electrolytes are the only known conditions in which genuine electrochemical N_2 reduction under standard temperature and pressure is reliably demonstrated to date, and the Li-mediated system is therefore the only benchmark system that can be used for this process[76,81,82]. Several generations of breakthroughs are still needed to enhance reaction kinetics and achieve viable photo- and (photo)electro-catalytic performances for commercial applications [124]. Advances in catalyst and electrolyte design are therefore required[125], but low product concentrations ($mass_{prod}$)[76,126] in these fields means a rigorous experimental protocol must be followed to ensure the integrity of reported experimental results.

The current goal in thermochemical NH_3 production is to decrease the temperature and pressure, enabling milder operational conditions compared to current Haber-Bosch plants[12]. However, lowering the temperature leads to an exponential decrease in the formation rate, which increases the possibility of contamination, particularly if the catalyst contains activated N. Also, the $mass_{prod}$ for these low-temperature

systems becomes so low that they fall below the $mass_{prod} > 2\ mass_{sys}$ threshold and are comparable to some of the more active electrochemical systems, necessitating isotope measurements. We note that the integrity of the reported formation rate must be rigorously evaluated especially at the low production points, because if the activity measurement is based on incorrect yields of NH_3, the error will propagate to the subsequent kinetic analysis.

[H2] Electro- and Photo(electro)-chemical Reactions

[H3] Reporting metrics of experimental results

To measure the catalytic performance, CA and/or CP measurements are carried out and the product concentration is determined, enabling a calculation of the yield and Faradic efficiency of the process. Typically, a metric such as the partial current density or formation rate is plotted as a function of applied current or potential, and the Faradaic efficiency is overlaid on a separate y-axis, displaying the maximum performance of the system (**Fig. 7a**)[79]. In photoelectrochemical systems, incident photon-to-current efficiency should be calculated utilizing a monochromatic light source[127]. All experiments should be repeated several times, from at least three independent batches of experiments to allow appropriate determination of a mean and its associate standard deviation. Representative CA or CP graphs should also be shown, as this illustrates the catalyst stability with time (**Fig. 7b**). In the case of powder photocatalysis, the amount of product formed should be plotted versus time and a production value per hour and gram catalyst can be extracted. The amount of product formed must be correlated with the amount of incident photons reaching the reaction vessel by calculating the average quantum yield **[G]** (or quantum efficiency), which is measured with monochromatic light sources or cut-off filters at a wavelength relevant to the monitored species[128,129].

As rigorous product detection is key to appropriately evaluating activity of (photo)electrochemical catalysts, product concentrations should be verified using at least two independent detection methods and quantitative agreement must be observed with each method over multiple points[130]. Typically, this strategy involves comparing results from colorimetric methods with results from isotope labelled experiments[76]. Ideally, the amount of product measured using appropriately cleaned $^{15}N_2$ (**Fig. 7c**) can reproduce the amount measured using $^{14}N_2$ quantitatively over numerous points, and a linear increase in detected product as a function of time or charge passed is observed (**Fig. 7d**).

[H3] Issues hindering progress in (photo)electrochemical N_2 activation

Reported yields and Faradaic efficiencies are very low for both electrochemical N_2 reduction and oxidation owing to the selectivity challenge and the activity issue. The reported partial current densities towards NH_3 are $\lesssim$ 1 mA cm $_{geo}^{-2}$ with up to 60% Faradaic efficiency. However, great care must be taken with experimentation to avoid false positives because NH_3 is ubiquitous in the environment[131] in concentrations similar to or greater than those reported. Many reports in **Fig. 6c** now include isotopic labelling experimentation (crossed points), which reflects the shift towards utilizing isotopes that has occurred over the previous 2 years[76]. Unfortunately, many of these reports only perform isotopic labeling in a single experiment[95,132–138], which does not demonstrate reproducibility as this is not enough to prove beyond doubt that synthesis of the product takes place. Also, the isotopically labelled gas typically contains $^{15}NH_3$ and $^{15}NO_x$ impurities[97], and most of these recent reports do not clean the gas prior to conducting the measurements, or if gas cleaning is reported it was done incorrectly[102]. Many of these reports are aqueous systems (non-asterisked), which typically suffer from low selectivity due to the competing H_2 evolution reaction[32] and could therefore be contaminated. The flagged Bi report[95] demonstrates the possibility of

inflated yield rates due to contamination: therefore researchers should reexamine high catalytic activity results via a rigorous experimentation[76,102] (see Experimentation). The Li-mediated system (denoted Li_xN/xx)[139,140] has recently gained renewed interest as it has proven effective via rigorous isotope sensitive experimentation[76]. This system is displaying comparatively increased partial current density towards NH_3[81], but it requires very negative potentials owing to the necessity of Li plating, making it energy inefficient.

For N_2 oxidation (squares, **Fig. 6c**), the partial current densities to NO_3^- are $\lesssim$10 μAcm^{-2}_{geo}[50], and the highest activity catalysts tend to correspond to $\lesssim$1% Faradaic efficiencies [56,141]. The field of electrochemical N_2 oxidation is novel and small, with only a handful of published papers [50–52,56,141]. However, there is hope of a significant increase in the selectivity because H_2 evolution is not a competing reaction to N_2 oxidation as it is for N_2 reduction. More theory to elucidate the reaction mechanisms is needed, along with a standardization and rigour regarding measurement, as the yields and product concentrations achieved are still very low.

In the case of photon-driven N_2 fixation, there is a general lack of rigorous testing[116]. The activity of titania is highly dependent on supplier, which has been attributed to differences in oxygen vacancy abundance[142] or carbon contaminants[143]. Nonetheless, there is an increasing number of reports of photochemical N_2 fixation on titania and numerous other materials[64,116]. Literature results in photochemical N_2 fixation must be viewed in the context of experimental rigour, which not only includes mere isotope labelling experiments but also tangible efforts to account for contamination sources, including the elimination of $^{15}NH_3$ and $^{15}NO_x$ impurities in gas streams. The necessity of isotope-labelled experiments is a consequence of the inherent measurement challenges, similar to those within electrochemical systems. For instance, some of the most widely utilized semiconductor photocatalysts for N_2 reduction are based on carbon nitride materials[144,145], which contain many amine terminal moieties and a generally high N content that can lead to producing meaningful amounts of NH_3 upon degradation[146]. Additionally, residual alcohols, amines and/or organic solvents can interfere with NH_3 quantification and result in an unreliable determination of NH_3 yields[116,147]. Photochemical studies in which isotope labelling shows quantitative agreement between $^{14}N_2$ and $^{15}N_2$ over multiple points (i.e. as a function of illumination time), along with proper gas cleaning to scrub away $^{15}NH_3$ and $^{15}NO_x$ impurities, have yet to be reported. Nonetheless, theoretical works suggest that photo-excited holes or electrons may facilitate N fixation more easily than metal electrodes, as the adsorbates at the electrodes may not be in equilibrium with the charge carriers[32].

[H2] Thermochemical N_2 Reduction

[H3] Reporting metrics of experimental results

The effects of temperature, pressure, and space velocity on catalytic activity as well as stability testing should be measured to evaluate a catalyst. The typical reports of catalytic performance are shown in **Fig. 8**. A temperature-dependent activity test within a certain temperature range (250-400 °C) should be conducted, and a benchmark catalyst (Cs-Ru/MgO) should also be tested under identical conditions. Special care should be given to the measurement of low-temperature activity (temperatures below 250 °C) as less product is formed due to lower activity, thereby being more prone to contamination issues and potentially not satisfying the criteria of $mass_{prod} > 2\ mass_{sys}$. For some of N-containing catalysts, such as nitrides, amides, imides and N-doped carbonaceous support, the catalysts should be reduced/pretreated under H_2 or H_2/N_2 at elevated temperature long enough to remove any reactive species from the catalyst. The stability is also crucial for evaluating the performance of a catalyst, and the activity data is only meaningful if there is stable performance. A life-time evaluation should show NH_3 production that is greater than the amount

of N in the system, and the NH_3 concentration should be greater than 100 ppm in the outlet gas. Isotope sensitive measurements are necessary if these production levels are not observed.

Kinetic measurements should be conducted under conditions far from the thermodynamic equilibrium and in the absence of mass and heat transfer limitations (**Fig. 8c**). The reaction rate is affected by the partial pressures of all gaseous components (N_2, H_2 and NH_3) as is shown in the power-law rate equation

$$r = kP_{NH3}{}^{\alpha}P_{N2}{}^{\beta}P_{H2}{}^{\gamma} \qquad \text{(eq. 8)}$$

where r is the reaction rate, k is the rate constant, P is the partial pressure of the reactants or product, α, β and γ are the reaction orders for NH_3, N_2 and H_2, respectively [148,149]. The reaction order of NH_3 (α) is obtained by measuring the NH_3 synthesis rates with varying total gas flow (F) at constant H_2 and N_2 partial pressures. The reaction order of NH_3 (α) could be obtained by plotting $\log(P_{NH3})$ (or $\log(C_{NH3})$, where C_{NH3} is the NH_3 outlet concentration) vs. $\log(1/F)$ where the slope is $1/(1-\alpha)$. For a step-by-step derivation, readers are referred to the Supplementary information.

For the reaction orders of N_2 (β) and H_2 (γ), $\log(r)$ plotted against $\log(P_{N2})$ would give a slope of β and $\log(r)$ plotted against $\log(P_{H2})$ would give a slope of γ provided that the partial pressures of the other gasses are kept constant. In cases where it is difficult to keep the NH_3 partial pressure (P_{NH3}) constant by changing the flow rate while varying either the N_2 or the H_2 partial pressure independently, one may determine β and γ by plotting $\log(r) - \alpha\log(P_{NH3})$ vs. $\log(P_{N2})$ or by plotting $\log(r) - \alpha\log(P_{NH3})$ vs $\log(P_{H2})$ (**Fig. 8c**) respectively, however it is a less desired solution (see derivation in the Supplementary Information). It is worth noting that the term $\alpha\log(P_{NH3})$ cannot be omitted unless α is close to zero or the partial pressure of NH_3 is kept constant. Calculating β or γ without accounting for NH_3 partial pressure variation may obtain inaccurate values of reaction orders and lead to a problematic interpretation of the reaction mechanism.

Generally, the N_2 order is positive and close to unity for the conventional oxide or carbon supported catalyst because the rate-determining step of these catalysts is the N_2 activation. However, H_2 and NH_3 orders can differ between various catalysts. For the iron-based catalysts, the H_2 order is positive and the NH_3 order is negative because of the strong adsorption of N[150,151]. In contrast, the H_2 order can be negative for some of the Ru-based catalysts due to the strong H_2 adsorption[152].

In theory, the apparent activation energy (E_a) should be determined by plotting $\ln(k)$ vs. $1/T$, rather than $\ln(r)$ vs. $1/T$ because the variation of NH_3 partial pressure has influence on the reaction rate according to the power-law rate equation. Thus, E_a should be measured at a constant NH_3 pressure. As shown in **Fig. 8d**, the apparent E_a values calculated at constant NH_3 pressure were greater than those determined at constant flow rate over $RuCl_3/\gamma$-Al_2O_3 catalysts[153]. The importance of NH_3 partial pressure should be considered in the kinetic measurements, as it could otherwise lead to inaccurate values. Moreover, we note the apparent activation energy is a complex function of both the activation energy for the rate-limiting step and the cost of freeing up sites. Thus, E_a cannot be directly compared to the activation enthalpy (nor the free energy) of the rate-limiting step.

[H3] Issues hindering progress in thermochemical N_2 reduction

Generally, catalysts operated at lower temperature are associated with a lower NH_3 synthesis rate. More recently, reactive catalytic materials have been employed for thermal NH_3 synthesis (**Fig. 6d**). Materials such as electrides[112], hydrides[78], nitrides[154] and oxy-hydrides[155] have been found effective in promoting/synergizing with transition metals, making early- and/or late-transition metals highly active. Some of the transition metal hydrides alone were also found to be catalytic active[156,157]. Those materials, however, have dynamic responses to the reacting environment. A recent neutron scattering investigation

reveals formation of H-containing species in the C12A7:e^- lattice under reaction conditions[158]. The TiH_2 shows the potential nitridation of the surface during the reaction[156]. The $VH_{0.39}$ is most likely converted into $VH_{0.44}N_{0.16}$ under reaction conditions, which is the stable active composition[157]. Amides, hydrides and nitrides of alkali/alkaline earth/rare earth metals can also react with H_2, N_2 and/or NH_3[159]. Moreover, catalyst made of coordination-unsaturated transition metal atoms or clusters may alter its chemical composition or physical state in response to the reacting environment. Characterization on a catalyst quenched by the reaction being evaluated would be more meaningful to provide information on the composition and chemical state of the active phase/site. However, this means of catalyst evaluation has yet to be fully addressed.

Adventitious N sources can also be significant when claiming catalytic activity with NH_3 concentration below 100 ppm or $mass_{prod} < 2\ mass_{sys}$. In addition to the possible sources of contamination discussed in electrochemical N_2 reduction/oxidation reactions, attention should also be given to reactive catalysts that would build up lattice or surface N species in situ under a N_2- or NH_3-rich atmosphere and elevated temperatures. Those N species have a chance to convert to NH_3 via a non-catalytic mechanism when the reaction condition allows for it, such as in an H_2-rich environment or at a low temperature. This conversion might result in a false-positive, which calls for using isotope labelling in the activity test for verification.

[H2] Reporting and interpreting DFT results

Quantum mechanical simulations, typically based on density functional theory **[G]** (DFT), are useful in understanding the mechanisms of N_2 activation. In this section, best practices in creating free energy diagrams, assessing active site stability and rationalizing free energy diagrams are discussed.

[H3] Creating free energy diagrams

To ensure the overall reaction energy is independent of the catalytic material when creating free energy diagrams, it is critical to ensure that the initial and final states correspond to gas-phase N_2 and gas-phase/aqueous products (for liquid-phase systems vapor pressure of N_2 can be used), respectively. For electrochemical free energy diagrams, a convenient model of applied potential is the computational hydrogen electrode (CHE) model[160], but more sophisticated models of applied potential may provide more accurate energies[161,162].

Considering the free energy of species, rather than only the energy obtained directly from DFT, is critical whenever computed energies are compared to experimental values[163]. At 0 K, the free energy consists of the energy obtained from DFT and the zero point energy **[G]**. The temperature-dependent free energy includes additional contributions from enthalpy and entropy, which can be computed through statistical mechanics (this standard DFT textbook[164] describes how each term is calculated). The entropy can be computed by assuming the adsorbate acts as a harmonic oscillator as an approximate upper bound. This assumption can lead to over-estimation in the case of low-frequency modes because the entropy diverges as frequency goes to zero for a harmonic oscillator, calling the need for rigorous treating and reporting of low-frequency modes[165]. Compared to the DFT energies, the inclusion of all free energy terms generally causes surface states to be less favorable due to the vibrational energy of the adsorbed states and the loss of entropy as they are bound to the surface. The entropy loss of a gaseous reactant as it becomes bound on the surface needs to be accounted for when in evaluating the free energy barrier[164] (**Fig. 2a**). The importance of the full consideration of all free energy terms is more concretely illustrated in **Fig. 9a**. The $*N_2H$ surface species gains 0.16 eV to be adsorbed on Ru (211) when considering only the DFT energy (grey). However, this $*N_2H$ surface species is destabilized by 0.67 eV due to the entropy loss relative to the gas phase and by

0.16 eV owing to change in the zero-point energy of the bonds (while it is stabilized by 0.05 eV from the enthalpy change), all leading to an energy penalty of +0.62 eV for *N_2H adsorption. This difference between DFT and free energies reveals that not considering the relevant free energy can lead to qualitatively incorrect conclusions of the thermodynamic driving force(s) for elementary reaction steps and what the rate-limiting steps are.

[H3] Assessing Active Site Stability

The feasibility of an active site model can be assessed in terms of at least two criteria: stability and reactivity. An active site's stability should be assessed by computing its surface energy using ab initio thermodynamics[160]. In general, activity and reactivity are related by a non-linear volcano plot relationship, where sites that are more reactive tend to be less stable. Therefore, it is necessary to find a trade-off between reactivity and stability[166,167]. An example of an activity-stability plot for surfaces toward O_2 reduction reaction on a number of Pt (111)-derived surfaces, where predicted current density represents activity and surface energy represents stability is shown in **Fig. 9b**. The most relevant surfaces form a Pareto-optimal frontier **[G]** along the activity/stability axes. Surfaces on the Pareto-optimal line represent optimal trade-offs between activity and stability, whereas surfaces below the line are sub-optimal, and surfaces further to the right are less stable and thus more challenging to generate under the atmospheric conditions used as the reference state. However, the stoichiometry of active sites can vary, and their relative stability will vary depending on the chemical potential of the environment. Therefore, it is critical to consider the relevant chemical potentials when assessing active site stability. Competitive adsorption is also an important component of active site stability. For example, analysis of N_2 adsorption free energy often assumes that there is no competitive adsorption from abundant spectator species such as *H, which may prohibit adsorption and reaction[73]. Surface phase diagrams provide a useful tool to assess stability and coverage of competing intermediates as a function of chemical potential[168].

[H3] Rationalizing free energy diagrams

When reading free energy diagrams, a distinction should be made between electrochemical steps and non-electrochemical steps. The thermodynamic barrier ΔG_{step}, which is the most uphill step in free energy along the reaction pathway, can be set as a lower bound for the true activation energy, $\Delta G^{\ddagger}$. As mentioned, a free energy diagram for electrochemical N_2 fixation with a thermodynamic barrier greater than ΔG_{step} = 1.5 eV under ambient conditions should be treated with skepticism.

Moreover, it is also important to consider the adsorption free energy of the inert N_2 molecule, an essential first step of N_2 fixation. N_2 physisorbing **[G]** to the surface results in an energy penalty of 0.67 eV[169] at 25 °C owing to the gas-phase entropy loss, and thus must be compensated by an enthalpic gain. To assess the point where N_2 adsorption becomes rate-limiting, collision theory can be used to obtain the rate of collisions between a gas and a surface[63]. Thus, the number of successful collisions per unit time per area becomes:

$$r \sim \frac{P_{N2}}{N_A\sqrt{2\pi m k_B T}} \exp\left(-\frac{\Delta G_{*\mathrm{N2}}}{k_B T}\right) \left[\mathrm{mol_{N2}\ cm_{geo}^{-2}\ s^{-1}}\right] \qquad \text{(eq. 9)}$$

where P_{N2} is the partial pressure of N_2, m is the mass of N_2 molecule, k_b is the Boltzmann constant, T is the temperature, N_A is the Avogadro constant, and ΔG_{*N2} is the thermodynamic N_2 adsorption free energy, which is a lower bound for the true adsorption barrier. To obtain the number of successful collisions per site per second, the rate can be multiplied by N_A and divided by the site density N_o.

$$r \sim \frac{P_{N2}}{N_o\sqrt{2\pi m k_B T}} \exp\left(-\frac{\Delta G_{*\mathrm{N2}}}{k_B T}\right) \left[\mathrm{s^{-1}}\right] \qquad \text{(eq. 10)}$$

Using a typical site density[63] of N_o = 1.5 x 10^{15} sites cm_{geo}^{-2} and 1 bar of N_2, the barrier corresponding to 1 successful collision per site per second (turnover frequency of 1 s^{-1}) becomes roughly 0.5 eV at 25 ºC. The collision rate can be estimated by using the concentration of dissolved N_2 at standard conditions (P_{N2}= 0.012 bar) with respect to aqueous solutions, in which case the N_2 adsorption free energy should be below 0.35 eV to ensure that N_2 adsorption is not rate limiting.

[H1] Applications

Electrochemical, photo(electro)chemical and thermochemical N_2 fixations have primarily been discussed in this Primer due to the size of interest and research efforts in these fields, and the possibilities they offer to sustainably produce high value N-containing chemicals. Particularly power-to-NH_3 is an attractive process, as NH_3 is the only other viable carbon-free green fuel to H_2 with significant advantages: it has ~70% higher H density than H_2 in liquid form, it can be liquefied under moderate conditions (20 °C at 0.86 MPa) for a more economical delivery, and it can be stored in benign, low-cost metal halide salts, which are mature, safe and reversible storage systems [170]. It can be used as fuel in gas turbines and power generators, or the NH_3 can be split, thereby providing a source of H_2 gas for fuel-cell based vehicles and marine transportation[171,172].

Centralized NH_3 production via the Haber-Bosch process is currently slowly replacing steam-methane reforming (Gen 1 NH_3) with wind or solar-powered water electrolysis to generate H_2 (Gen 2, **Fig. 1**)[28]. Gen 2 facilities would significantly reduce the carbon footprint of NH_3 production[12]. Thermochemical N_2 reduction is a crucial key point, as lowering the required pressure and temperatures of the Haber-Bosch process enables smaller and thereby cheaper production facilities[11]. For fully decentralized NH_3 production, such that there would be one device per farm for fertilizer production, significant breakthrough in electrochemical or photo(electro)chemical N_2 activation (Gen 3, **Fig. 1**) is necessary[173]. These advanced processes could significantly reduce the dependence on Haber-Bosch on a local scale, as the only inputs should be air, water and renewable electricity on a small-scale device. Breakthroughs on the small-system scales (on the order of 1 device per farm or greenhouse) would also lead to electricity storage as NH_3, aiding the intermittency issue of renewable electricity sources, and more advances in overall power-to-X technologies, as more infrastructure and reliance on Gen 3 NH_3 will increase understanding of general electricity conversion, energy storage, and reconversion pathways.

Furthermore, N_2 activation has widespread use across many different fields, as N-containing chemicals is pivotal in the pharmaceutical industry, the synthesis of polymer materials, dye manufacture, and the field of organic synthesis[174]. Direct synthesis of compounds such as urea[175], the most commonly used and highest N-containing solid fertilizer by weight, via electrochemistry from N_2 and CO_2 in H_2O would skip the intermediate step of NH_3 synthesis coupled with further processing, enabling decentralized production of a high-value chemical. One could even dream of direct electrochemical synthesis of higher complexity N-containing compounds, such as acetonitrile, pyridines, amino acids, etc.[11]. Understanding N_2 activation as the critical first step can therefore tremendously impact the chemical and pharmaceutical industry.

[H1] Reproducibility and data deposition

[H2] The importance of reproducibility

Ensuring complete account and mitigation of contamination sources is key to improving reproducibility in N_2 activation. Given the ubiquity of N-impurities, results of catalytic performance must be accompanied with experimental details showing how contamination sources have been mitigated. To this end, performing complete isotope-labelling experiments, with time-dependent product quantification and proper cleaning of

the $^{15}N_2$ gas stream, is imperative to ensure unambiguous certainty of successful N_2 fixation. Additional rigor needs to be applied when performing electrochemical and photo(electro)chemical measurements and detecting product formation from these processes, especially when the reported selectivity is very low. For electrochemical measurements, the pre- and post-test Ohmic resistance can differ substantially (See Experimentation) such that the shift in potential should be properly adjusted[76]. Similarly, in thermochemical studies, catalyst preparation-pretreatment and activity measurements are two main factors influencing the reproducibility of the experiments, so reporting the associated experimental details is imperative.

The reported data should highlight $n \geq 3$ reproductions, which include at least three repeated measurements in product detection for each catalytic activity point, three independent activity tests, and three independently prepared catalyst batches. The mean and spread of each data point must be reported, acknowledging errors from activity measurements and product detection, with the appropriate number of significant digits. This is significant as several studies report an excessive number of digits beyond the precision usually attainable in catalysis.

[H2] Data deposition and reporting

Transparency in reporting and data deposition are essential. Useful figures of merit regarding the catalytic performance and details of the experimental conditions, as elaborated in **Table 2**, must be reported to enable a thorough assessment of the experimental rigor and aid comparisons of data collected under different conditions. Ultimately, these efforts are aimed at evaluating the product mass relative to the system size of the experiment. Kinetic measurements such as the determination of reaction orders and activation energy may be required according to the need of these mechanistic details. Lastly, pre- and post-measurement (and/or in situ) characterization of the catalyst may be necessary to ascertain changes associated with the reaction conditions.

In a move towards open data, raw calibration and test data associated with catalytic activity measurements should be openly shared, also including the relevant data analysis scripts where possible, and results such as converged atomic coordinates and vibrational frequencies when a DFT calculation is performed.

[H1] Limitations and Optimizations

[H2] Cost of isotope experiments

For repeated isotope labelled experiments, the cost of $^{15}N_2$ can be prohibitively expensive, as a single long-term experiment can easily cost upwards to 2,300 USD for 5 L. This high cost can be circumvented by introducing a glass circulation pump. Once a high enough $^{15}N_2$ atmosphere is achieved in the system, the glass pump will continuously circulate the gas, without the need to supply more throughout the experiment. Furthermore, the circulation pump has the added benefit of not introducing contaminants over time, if the gas stream contains any NH_3 or NO_x species, decreasing the possibility of false positives. The glass circulation pump can be made in-house[176] as seen in **Fig. 10a**, or purchased commercially.

Isotopically labelled $^{15}N_2$ can contain significant amounts of both $^{15}NH_3$, and $^{15}NO_x$ species that reduce easily, leading to isotopically labelled contamination[97]. We do not advocate the use of aqueous solutions to clean N_2, as they would not trap all contaminants[177]. The residence time of the bubbles compared to the diffusion time inside the bubbles would need to be ideal, with a certain probability of uptake. The bubbles need to be tiny, so they rise slowly and have fast internal mixing and large surface/volume ratio[102]. Furthermore, it is unclear how NO_x species would be trapped in acid[134]. We found that a home-made reduced Cu catalyst combined with a freeze trap to be efficacious for removing impurities, on the basis of the measured level of all NH_3 and NO_x impurities removed before and after the cleaning[76]. The reduced Cu catalyst will catch all NO_x species, while the cold trap freezes out NH_3. Commercial gas purifiers down to

parts per trillion per volume fraction (pptV) level are also available for purchase. A complete home-built and inexpensive system for both the glass circulation pump and the reduced Cu catalyst is shown in **Fig. 10b**.

[H2] Access to NMR

NMR is the most commonly reported technique for isotope labelling experiments, as it can distinguish between $^{14}NH_3$ and $^{15}NH_3$. Not all will have access to a high-field 800 MHz NMR, but the use of the more commonly available 400 MHz NMR can achieve similar sensitivity, covered in more detail in REF[76].

[H3] Overcoming mass-transport limitations

Mass-transport of N_2 to the catalyst surface is one of the main limitations in electrochemical and photo(electro)chemical systems. However, using a gas diffusion electrode (GDE) in a flow-cell system creates triple-phase (solid, liquid and gaseous) boundary points where N_2 is readily available for reaction at the surface of the electrode, which can help circumvent this limitation. Using this GDE is advantageous over the more common H-cell or single compartment cells that rely on N_2 solubility in the electrolyte, which is typically quite low for most liquids[178]. For the electrochemical Li-mediated N_2 reduction in an H-cell[81], the equivalent flow-cell system has been proven to significantly increase the Faradaic efficiency and current density via application of a slight overpressure on the backside of the GDE[80].

[H1] Outlook

[H2] Adoption of standardized test protocols

N_2 reduction and oxidation at low temperature and pressure are reactions with immense technological significance. Unfortunately, much published research lacks rigorous and standardized testing, leading to possible contamination and false positives. The possibility of contamination is particularly prominent for reports with low product formation rates, spanning all electrochemical and photo(electro)chemical systems to date, as well as some low temperature thermochemical systems. The only conclusive proof of productive N_2 activation is via repeated and quantified isotope labelled testing coupled with proper gas cleaning. In this Primer, the cut-off necessitating the use of the crucial $^{15}N_2$ quantitative isotope labelling experimentation for all N_2 activation reactions has been defined; both $mass_{prod} > 2\ mass_{sys}$ ($mass_{sys}$ is based on experimentally measured N in the system) and C_{prod} >100 ppm must be satisfied. This defined caliber should prevent reporting false positives, which hinder development of the N_2 activation field.

Beyond electrochemical, photo(electro)chemical and thermochemical systems, efforts on non-thermal plasma N_2 fixation have been pursued in recent years[179]. Generally, the plasma-driven N_2 fixation studies report product concentrations of hundreds of ppm and up to ~5% of the gas stream[36], dwarfing the detrimental contribution of labile N-species from various contamination sources. However, with the field's primary focus on achieving higher energy efficiency, several studies using dielectric barrier discharges as the most common plasma source show worryingly low NH_3 production (C_{prod} <100 ppm)[35], possibly dipping into the range of contaminants. The mechanochemical method of NH_3 synthesis has also emerged as a new direction for N_2 activation[39,40], with similarly high reported NH_3 yields, but the field can benefit from the critical assessment of the potential size of N-contaminants. Researchers in these exploratory areas should adapt the protocol in this Primer by comparing the product mass with the system size and performing quantitative isotopic-labelling verification technique at the low-yield data points.

[H2] In situ mechanistic insight

Insight into the reaction mechanisms on N_2 reduction has largely been built on theoretical investigations[69,73,180]. In-situ and in-operando techniques to probe intermediate species can validate or challenge established paradigm, and provide valuable considerations for future catalyst designs. In **Box 2**,

we discuss four techniques which can be utilized for electrochemical and thermochemical N_2 activation, but other spectro(electro)chemical techniques such as Differential Electrochemical Mass Spectrometry (DEMS) among others in development may be useful. All of these techniques can be complemented with Raman and core-level spectroscopies to gain an understanding of the underlying mechanistic processes enabling N_2 activation. However, adoption of the rigorous protocol takes precedence to ensure what is being detected is not associated with the presence and redox processes of adventitious N sources.

[H2] Commercialization

The reported false positives and likely unreliability of many prior publications in N_2 fixation have undoubtedly affected the reputation of the field. In the immediate future, the scientific community should aim to restore the field's integrity and eliminate the emergence and propagation of unreliable results. An increase in rigor of experimental practices, efforts to reproduce reported results, cross-pollination of knowledge and best practices across laboratories, and a more deliberate regard toward fundamental concepts and principles will support this restoration.

In the next 5-10 years, we anticipate researchers will focus on addressing the field-specific needs (**Box 3**), ultimately finding breakthrough catalysts with practically relevant and reliably demonstrated yield rates, selectivity, stability and energy efficiency to enable industrial deployment of sustainably-produced NH_3. The obsessive pursuit of breakthrough results must go hand-in-hand with robust fundamental studies to identify reaction mechanisms, active sites and reaction kinetics, aided by experimental mechanistic studies and quantum chemistry or other computational methods. Ultimately, concerted efforts from experimental and theoretical communities will be key to discovering practical solutions to decarbonize the activation of N_2.

Boxes

[bH1] Box 1. Sources of system N mass

[bH2] $mass_{N,cat}$

The amount of measured N in the catalyst and support, which must be experimentally determined. This measure is important, even if the catalyst does not intrinsically contain N, as substantial levels of NO_3^- and nitrides can contaminate commercial metal sources[107,181,182], despite manufacturer's claims otherwise. The simple 2-step procedure of alkaline and acidic treatment of the catalyst should be conducted, followed by HPLC or UV-vis analysis or any equivalent method for determining N-content.[182] Special care should be taken regarding N-buildup on the catalyst if pretreated with an N-containing procedural step. These N-species could contaminate the catalyst, and convert to NH_3 via a non-catalytic route[183,91]. Therefore, examining the N-content of the catalyst as bought, after any pre-treatment, and after catalysis should be a routine practice. If the N-content of the catalyst is not experimentally determined, one should consider $mass_{N,cat}$ as at least 25% of the whole mass of the catalyst, unless the catalyst is intrinsically N-containing (for example, a nitride), in which case 100% of the mass should be considered.

[bH2] $mass_{N,electrolyte}$

The measured amount of N in the electrolyte. Electrochemical and photo(electro)chemical systems submerge the catalyst in electrolyte, and if the electrolyte itself contains N species, these must be considered as sources of contamination, owing to possible electrolyte breakdown. However, the electrolyte itself may also be contaminated, as chemicals and membranes (for example, Nafion) readily soak up NH_3 from the surroundings[76], and both NO_x and NH_3 blank measurements of the electrolyte should be included with each batch of electrolyte.

[bH2] $mass_{N,absorber}$

The measured amount of N in the photoabsorber present in photo(electro)chemical system. This may contain sources of activated N as a contaminant, which should be determined experimentally.

[bH2] $mass_{N,gas}$

The total calculated N impurities of the N_2 gas stream[97,102]. If the purity of the N_2 is 99.999%, one must consider 0.001% of the total gas used to be entirely contamination, and calculate the mass of this based on flow rate and duration. Alternatively, a proper gas cleaning procedure, with reported NH_3 and NO_x contamination of the gas before and after cleaning can be used.

[bH1] Box 2. In-situ and operando techniques for N_2 fixation

[bH2] Surface enhanced infrared spectroscopy (SEIRAS)

SEIRAS can detect the adsorbates in electrochemical N_2 fixation in operando. The infrared adsorption peaks can be attributed to vibrational modes of reaction intermediates, and these signals can be enhanced on metal surfaces by the SEIRA effect (enhancement of infrared adsorption as a result of enhanced optical fields on a surface [184]. Several studies have attempted SEIRAS for electrochemical N_2 reduction[185,186], but contributions from contamination to the detected species are highly probable. Nonetheless, successful in-situ Fourier transform infrared (FTIR) spectroscopy for electrochemical NH3 oxidation on Pt electrode has been reported187. Here, various bands, detected at different voltages, were ascribable to the HNH bending mode of *NH3, NH2 wagging mode of $*N_2H_4$, absorption of NO bridged species and HOH bending mode of *OH groups.

[bH2] Electron Paramagnetic Resonance Spectroscopy (EPR)

EPR allows the monitoring on paramagnetic species - having unpaired electrons - as a function of potential in an electrochemical process, detectable upon rapid freezing of the electrodes. EPR spectra have detected nitrous oxides in redox processes in biomolecules [188] and during alcohol oxidation.[189]. Electrochemical EPR could detect absorbed paramagnetic surface-adsorbed NO (*NO) species formed during N_2 oxidation.

[bH2] N_2 isotopic exchange reaction (N_2-IER)

N_2-IER ($^{15}N_2 + {}^{14}N_2 \rightarrow 2{}^{15}N{}^{14}N$) has been used to probe the reaction mechanisms and the rate-determining step of the thermochemical NH_3 synthesis, by introducing $^{14}N_2/^{15}N_2$ gas mixtures and monitoring the $^{14}N_2$, $^{15}N_2$ and $^{14}N^{15}N$ gas phase composition. Examples confirming N_2 dissociation as the rate-determining step using N_2-IER for NH_3 synthesis have been reported on Fe[190] and Ru[191,192]. A N_2-IER study on cobalt molybdenum nitride[193] demonstrates the possible participation of lattice N in a Mars-van Krevelen mechanism involving the hydrogenation of lattice N to evolve NH_3, and the refilling of lattice N vacancies by N_2 gas[194].

[bH2] Steady State Isotopic Transient Kinetic Analysis (SSITKA)

SSITKA is performed under steady-state conditions and involves introducing a step change in the isotopic content of the reactant and monitoring the transient responses of the isotopically labeled species[195]. SSITKA has been used to study the kinetics of NH_3 synthesis on commercial Fe[196] and Ru[197–200] catalysts. A study on commercial Fe catalysts reveals *N as the most abundant reactive intermediate[196]. The role of potassium promoter over Ru catalysts, investigated by SSITKA, is revealed to induce surface site heterogeneity on Ru/SiO_2, creating super-active sites responsible for enhanced catalytic activity[197].

[bH1] Box 3. Field-specific progress, needs, and insight

[bH2] Thermochemical N_2 reduction

The thermochemical N_2 reduction is the most advanced in terms of technological readiness, as there are a variety of newly developed catalysts shown to produce NH_3 at low pressures (1-10 bar) and low temperatures (< 300 ^oC). However, higher operation temperatures (compared to ambient conditions) and pure H_2 as the feed gas are still required, necessitating an additional H_2 cleaning step. Therefore, major efforts include exploring unconventional, highly active and electron-rich materials as catalysts or catalyst supports to optimize the reaction rate and decrease the temperature further. Elucidating the active site and reaction mechanism should also be a focus area. Any progress in fundamental insight and/or practical transformation in thermochemical NH_3 synthesis would have a profound impact on the field of heterogeneous catalysis.

[bH2] Electrochemical and photo(electro)chemical N_2 reduction

The requirements for high yields comparable to the Haber-Bosch process or even to thermochemical systems are not necessary, as the focus is on creating completely decentralized systems[28]. Unfortunately, the validation of aqueous results using rigorous protocols[76,102] is necessary in light of the sheer selectivity challenge in aqueous environments and the ubiquity of contaminants. Once these systems are experimentally validated, efforts towards increased catalytic activity, selectivity and number of active sites can be considered[125].

The non-aqueous Li-mediated N_2 reduction process is proven to work, achieving record high energy efficiencies[79–82]. However, a vast majority of the reported literature still remains focused on aqueous systems (**Fig. 6**), which is most likely due to the numerous experimental challenges for non-aqueous systems, such as Ohmic drop compensation and high over-potentials, evaporation of organic solvents, compatibility of colorimetric methods, etc. Furthermore, this system has significant kinetic challenges due to mass-transport limitations that need to be overcome, which is possible with the use of GDEs in flow-cell type systems (see Limitations and Optimizations). Further research in these systems would enable scientists to tackle these challenges as breakthroughs occur, thereby increasing the feasibility of the system for practical commercial use.

[bH2] Electrochemical N_2 oxidation

Electrochemical aqueous N_2 oxidation is piquing the curiosity of the scientific community. Nonetheless, this field is in its infancy, with ample opportunity for fundamental insight and step improvements to catalyst performance.

Tables

Table 1 Electrochemical and photo(electro)chemical systems contaminations sources and solutions. Methods adapted from Liu et al.[107]

Sources of Contamination	**Nitrogen form**	**Method of Elimination**
Feed gas[97]	NO_x, N_2O and NH_3	Use of home-made reduced Cu catalyst and a freeze trap, or commercial gas purifier.
Impurities in the catalyst[91,181,182]	NO_x^- and NH_4^+	Complete removal via pre-reduction of the catalyst before N_2 reduction testing.[107]
Uptake/release from the membrane[76,106,107]	NH_3	Replace with contamination-free membrane, such as Celgard[107].
Electrolyte	NH_4^+, NO_2^- and NO_3^-	Removal via annealing of electrolyte salt or other cleaning methods.[107]
Glassware, tubes, laboratory air, etc.[201]	NH_3	Ensure the entire system is properly cleaned between uses; by boiling in ultra-pure water and drying in oven.

955 **Table 2. Required reporting standards for catalyzed N_2 reduction and oxidation.**

Data type	Definition	System type
Reporting of catalyst performance		
Yield rate	Amount of product formed in a given time interval.	All systems
Area-normalized activity	Yield rate normalized to either geometric or electrochemically active surface area.	Electrochemical
Mass-normalized activity	Yield rate normalized by the mass of catalyst.	All systems
Turnover frequency	Rate of chemical conversion normalized to number of actives per unit of time.	All systems
Faradaic efficiency	Ratio of charges employed for the synthesis of a given product relative to the total amount of charge passed through the circuit.	(Photo)electrochemical
Stability	Capability of a catalyst to perform in prolonged time intervals without detriment in its intrinsic activity	All systems
Energy efficiency	Ratio of converted energy relative to the initial energy input.	All systems
Average Quantum yield	Ratio of electrons transferred towards product relative to the incident photons reaching the sample at a given wavelength.	Photo(electro)chemical
Incident photon-to-current efficiency	Ratio of produced photocurrent versus the incident photon flux at a given wavelength.	Photo(electro)chemical
Reaction orders	The power dependence of reaction rate on reactant concentration.	All systems
Activation energy	The minimum amount of energy required to activate reactants to a state in which they can undergo a chemical reaction.	All systems
Reporting of experimental conditions		
Catalyst loading	Mass of catalyst employed in a single experiment.	All systems
Gas purity & flow rate	Purity and flow rate of the $^{14/15}N_2$, H_2 and Ar gases.	All systems
Time	Length of time of the experiment.	All systems
Potential	The operating potential of working electrode during reaction.	Electrochemical
Electrolyte volume	The volume of the supporting electrolyte used in electrolysis.	(Photo)electrochemical
Temperature and pressure	The temperature of the catalyst bed and the total pressure of the reaction gases.	All systems
Photon intensity	Photon flux reaching the sample per second and illumination area.	Photo(electro)chemical
Illumination area/distribution	Available surface for the incident photon flux to reach the sample.	Photo(electro)chemical
Weight hourly space velocity	Flow rate of the reaction gas fed to the reactor, divided by the mass of catalyst.	Thermochemical (most relevant)
Essential Information		
Gas cleaning procedure	An account of how impurities are removed in the gas streams.	All systems
Technical specifications of materials	Details such as manufacturer and purity of commercial catalyst and reagents used in catalyst synthesis; purity of electrolytes and ionic salts; additive content (for non-organic solvents).	All systems
Key experimental details	Details such as the use of glovebox during electrolysis, cleaning of system impurities, solvent-handling (drying steps), and residual water traces (non-aqueous systems).	(Photo)electrochemical
Catalyst characterization	Structural or chemical information pre- and post- catalytic measurement to inform changes to the catalyst.	All systems

Figure Captions

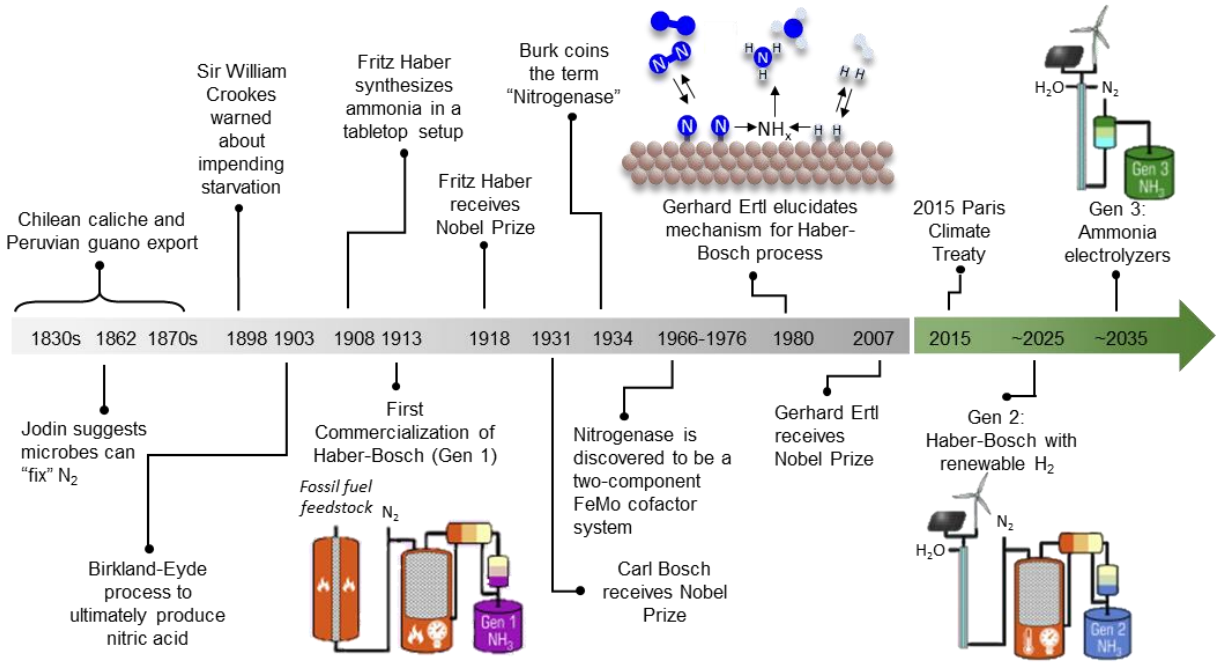

Fig. 1. **Historical development of N_2 activation.** Nature mainly produces activated N-species via the nitrogenase enzyme[6]. The source of N-containing fertilizer first originated from caliche deposits and guano, both predicted to be unsustainable[8]. Two commercial N_2 activation processes emerged in early 20th century: the Birkland-Eyde and Haber-Bosch process, and the latter has since dominated the N_2 activation industry[7], with 3 Nobel prizes given for its discovery[14]. With the global commitment to tackle climate change, the decarbonization of N_2 fixation is envisioned to involve two technology generations: coupling the Haber-Bosch process with renewable H_2 (Gen 2) and electrochemical NH_3 synthesis (Gen 3)[28]. Components coloured orange represent process steps requiring elevated temperatures. Schematics of Gen 1, 2 and 3 technologies were adapted with permission from REF[28], Elsevier.

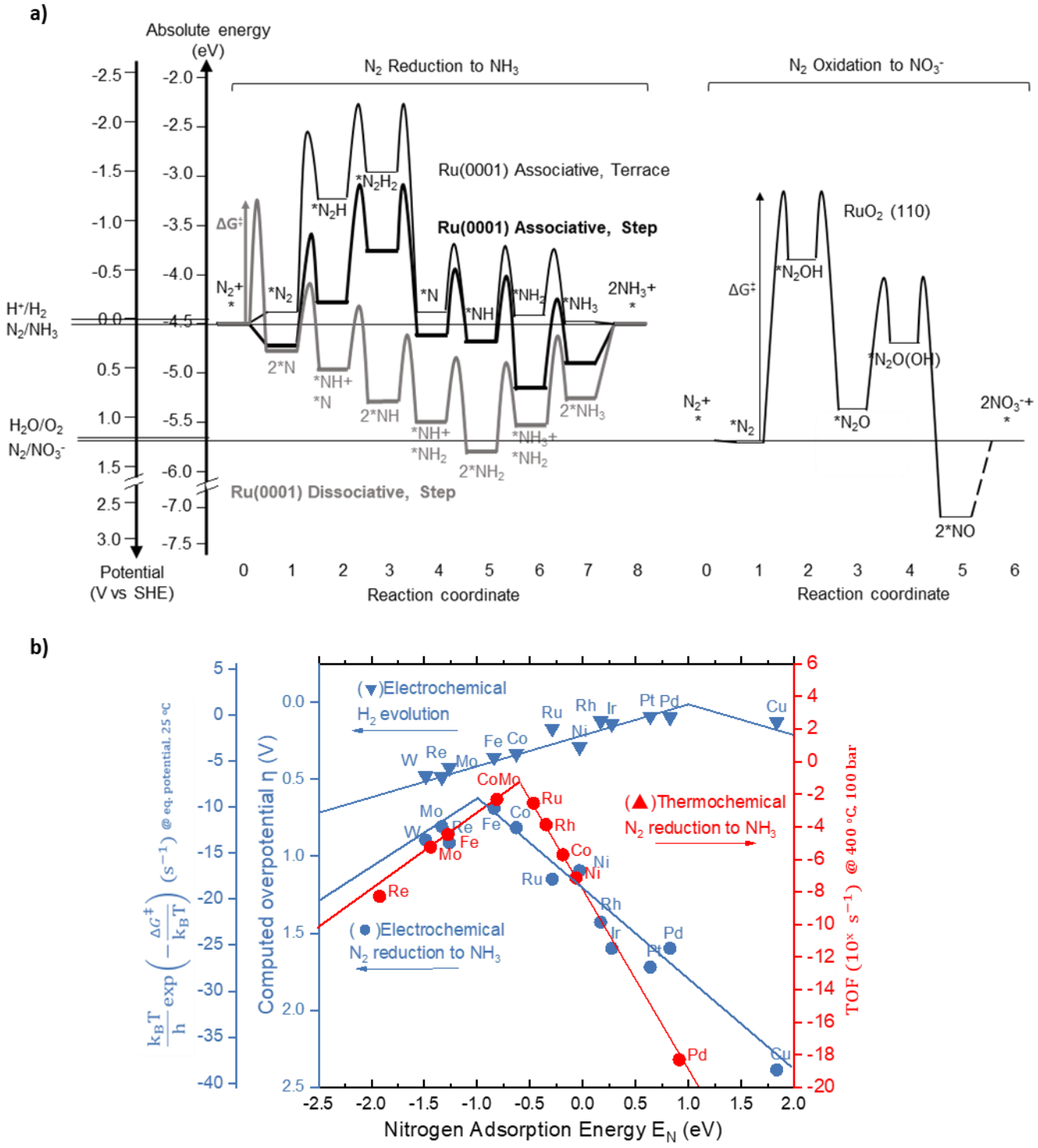

967

968 **Fig. 2. The fundamental challenges of N_2 activation.** a) Standard equilibrium potentials for N_2 and H_2O
969 redox are aligned with the electron energy (0 V_{SHE} equals -4.44 eV on the absolute scale where electron in
970 vacuum is 0 eV[42]). The free energy diagrams for N_2 reduction[74] and oxidation[56] on selected surfaces are
971 plotted at the equilibrium potentials referenced to standard conditions, 1 bar $NH_{3(g)}$ and 1M $H^+NO_3^-{}_{(aq)}$. *X
972 refers to surface adsorbed intermediates. The energy difference between two states (for example, step

1-2 of associative N_2 reduction) corresponds to the thermodynamic barrier and can be lowered by applying potential if the step involves an electron transfer. An additional activation barrier may be present, shown as bumps between steps, whereby the value 0.7 eV is chosen for all coupled proton-electron transfer steps (consistent with Singh et al[66]). The N-N dissociation barrier follows ref[202] in which the zero-point energy and the gas phase entropy loss of N_2 have been included. The overall reaction barrier can be approximated by the step with the highest barrier ($\Delta G^{\ddagger}$), which is much slower than other elementary steps thus governing the rate. b) Limiting potential analysis[66] (blue) for electrochemical N_2 reduction and H_2 evolution (overpotentials referenced to $N_{2(g)}/NH_{3(g)}$ and $H^+_{(aq)}/H_{2(g)}$ standard potentials) as a function of N binding energy on transition metal terraces. For electrochemical N_2 reduction, $N_2+*+H^++e^- \rightarrow *N_2H$ (Step 0-2 in panel a) and $*NH+H^++e- \rightarrow *NH_2$ (Step 5-6) define the right and left legs respectively. For H_2 evolution, $*+H^++e^- \rightarrow *H$ and $*H+H^++e^- \rightarrow H_2$ define the right and left legs. The rate constants are shown in the second blue axis, where k_BT/h equals 10^{13} at 25 °C. The red points correspond to the calculated turnover frequencies (TOF) on transition metal FCC/HCP (211), computed using a micro-kinetic model by considering the dissociative mechanism as described in ref[69]. The synthesis condition is 400 °C, 100 bar, gas composition H_2:N_2 =3:1 containing 5% NH_3. The N_2 reduction energy diagrams in panel a were adopted with permission from REF[74], Royal Society of Chemistry, and the N_2 oxidation diagram with permission from REF[56] , Wiley. In panel b, the electrochemical N_2 reduction and H_2 evolution plots are adapted with permission from REF[66], Elsevier and adapted with permission from Singh, A. R. *et al.* Strategies toward Selective Electrochemical Ammonia Synthesis. *ACS Catal.* **9**, 8316–8324 (2019). Copyright 2019 American Chemical Society. The turnover frequency data points for thermochemical N_2 reduction are reproduced with permission from REF[69]

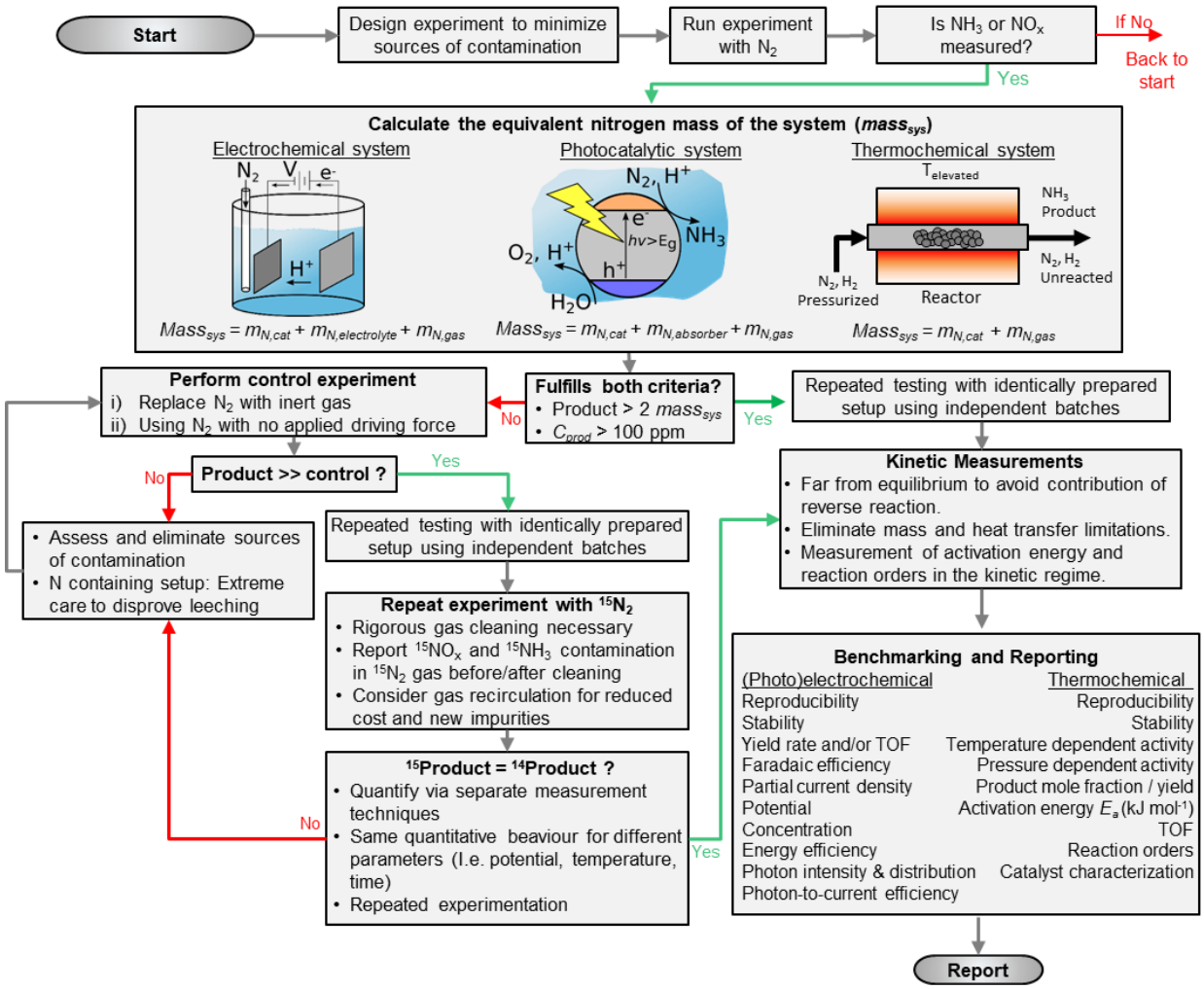

Fig. 3. General flow chart of experimentation. The total equivalent mass of the system, $mass_{sys}$, must be determined, which will be compared with the amount of product (NH_3 or NO_3^-) measured, $mass_{prod}$, in order to determine the need for isotope labelled experiments. The $mass_{sys}$ is the summation of the relevant N-containing masses, which includes the experimentally measured N in the catalyst ($m_{N,cat}$), the mass of N in the electrolyte ($mass_{N,electrolyte}$), the mass of the N-containing absorber ($mass_{N,absorber}$), and the calculated or measured mass of impurities in the gas stream ($mass_{N,gas}$).

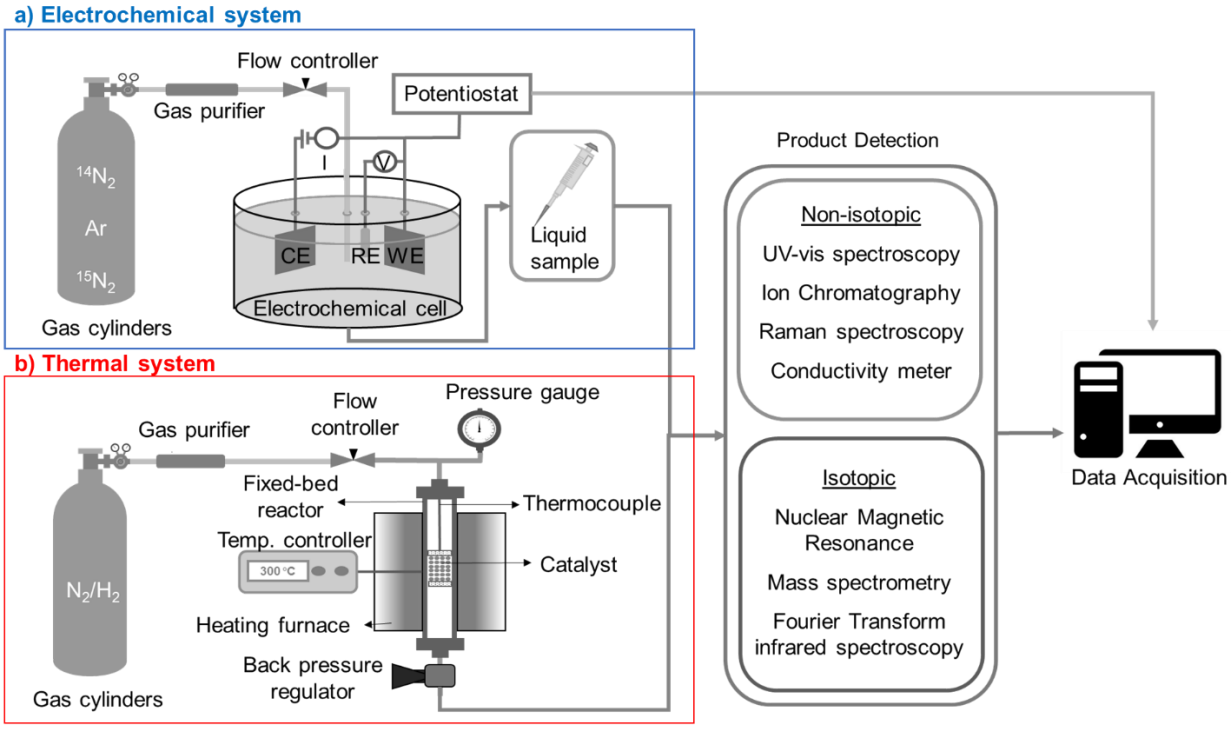

Fig. 4. Experimental setup for electrochemical and thermochemical N_2 activation. a) Experimental setup for electrochemical N_2 reduction or oxidation reactions. The gas passes through a gas cleaner (either a reduced metal catalyst and freeze trap, or a commercial purifier), then flows into the electrochemical cell with a defined flow rate. The setup can be adapted for photoelectrochemical systems by using a photoelectrochemical cell with an illumination source. The reaction of interest is undertaken by controlling the potential across the electrodes via a potentiostat. For photochemical systems, the setup does not require a potentiostat, and the cell typically contains a suspension of particles or a surface with the active catalyst, and an illumination source is used to drive the reaction. b) Activity measurement system for thermal NH_3 synthesis. The setup contains a fixed-bed reactor, a furnace with a temperature controller, a thermocouple placed on the top of catalyst bed, gas purifiers, a flow meter, a pressure gauge and a back-pressure regulator. Then, the product of catalysis is detected via either non-isotope or isotope-sensitive techniques if necessary.

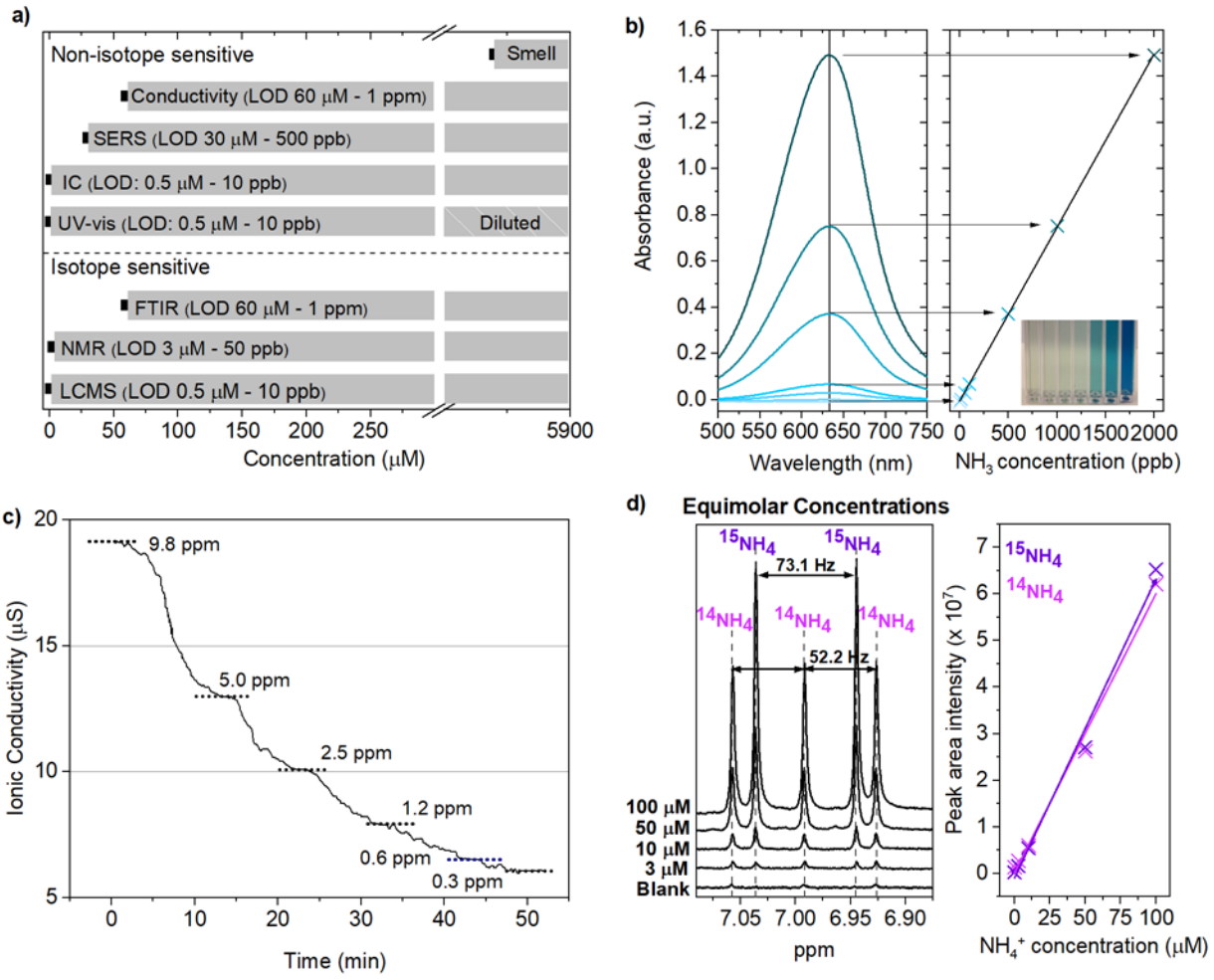

Fig. 5. Isotopic and non-isotopic NH_3 detection methods. a) Detection limits of well-known techniques for NH_3 quantification. The bar at 5882 µM (100 ppm) corresponds to NH_3 concentrations in liquid where olfactory detection is possible beyond any doubt[96]. UV-vis[76], Conductivity meter[120], and nuclear magnetic resonance (NMR)[76] is discussed in text, Fourier transform infrared spectroscopy (FTIR)[83], liquid chromatography mass spectroscopy (LCMS)[203], surface enhanced Raman spectroscopy (SERS)[204] and ion chromatography (IC)[205] is discussed in the Supplementary Information. b) UV-vis spectra of indophenol blue method, showing quantification via calibrated samples from 10 to 2000 ppb NH_3 in H_2O. Straight line is fitted based on peak absorbance of each sample, displaying linearity with sample concentration[206]. c) Conductivity measurement curve showing sensitivity of the NH_3 concentration from 9.8 to 0.3 ppm in purified H_2O[207]. Due to the intensity of the conductivity baseline, it is difficult to detect an NH_3 concentration below 1 ppm. d) Example of NMR spectra of increasing equimolar $^{14}NH_3$ and $^{15}NH_3$ concentrations, clearly showing the respectively distinct triplet and doublet peaks. Calibration curve for $^{14}NH_3$ and $^{15}NH_3$ based on area under peaks, respectively, the triplet and doublet peaks from the NMR spectra[76]. Panel c is reprinted with permission from REF[207], Elsevier. Panel d is reprinted from REF[76], Springer Nature Limited.

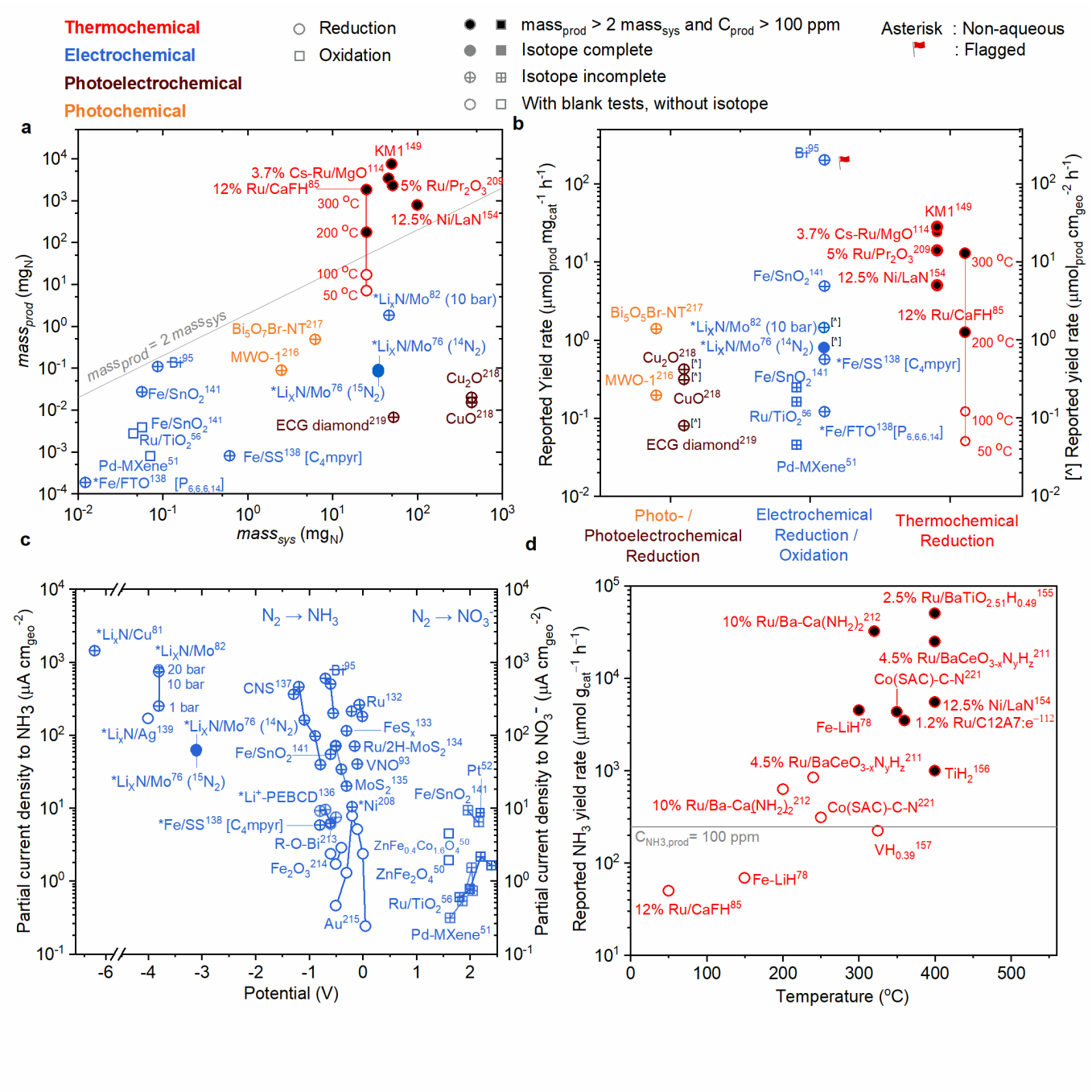

Fig. 6. State-of-the-art literature overview of electrochemical, photo(electro)chemical, and thermochemical N_2 activation. Evaluation of experimental conditions for thermochemical (red), electrochemical (blue), photochemical (orange), and photoelectrochemical (brown) N_2 fixation. Experimental details can be found in **Table S1-3**. Circle represents reduction, square represents oxidation. Unfilled symbol represents data with simple background tests. Cross represents data with either qualitative or quantitative isotope labelled experiments at a single point, without measuring or cleaning gas contaminants. Filled symbol represents repeated isotope labelled experiments with rigorous gas cleaning. Black-filled data satisfy both $mass_{prod} > 2mass_{sys}$ and $C_{prod} > 100$ ppm. Asterisked points contain non-aqueous electrolytes. Flagged data raise suspicion of contamination based on non-reproducible results. a) Comparison of $mass_{prod}$ with $mass_{sys}$ for different catalytic systems. $mass_{N,cat}$ is calculated based

on 25% catalyst weight for non-N-containing catalysts, and 100% for N-containing catalysts. Thermochemical data at 400 °C and 1 bar unless otherwise specified: Cs-Ru/MgO[114] at 9 bar, Ru/Pr_2O_3[209] at 390 °C and 9 bar, KM1[149] at 10 bar. b) Comparison of reported mass-specific activity. Yield rates of data points annotated by [^] are expressed in µmol cm_{geo}^{-2} h^{-1}. c) Literature overview of partial current density towards NH_3 (left y-axis) or NO_3^- (right y-axis) from product detection as a function of potential vs RHE, unless otherwise specified. Fe on Stainless Steel (Fe/SS) and Fe/FTO[138] reported vs NHE, Li_xN/Cu[81] total cell potential with Ohmic correction, Ni[208] vs Ag wire in 0.1 M LiCl/EDA, Li_xN/Ag[139] is vs Ag/AgCl/AgCl (sat), LiCl, $LiClO_4$/THF reference. d) Literature overview of thermochemical NH_3 synthesis catalyzed by "reactive" materials whose composition or active phase may change during or after reaction. The line $C_{NH3\text{-}prod}$ = 100 ppm was calculated with the assumption of WHSV= 60,000 ml g_{cat}^{-1} h^{-1}. Data at 10 bar unless otherwise specified: Ru/CaFH[85] at 1 bar, TiH_2[156] at 50 bar, 2.5%Ru/$BaTiO_{2.51}H_{0.49}$[155] at 50 bar, 4.5%Ru/$BaCeO_3$-xN_yH_z[211] at 9 bar, Ru/Ba-$Ca(NH_2)_2$[212] at 9 bar, 12.5%Ni/LaN[154] at 1 bar, $VH_{0.39}$[157] at 50 bar.

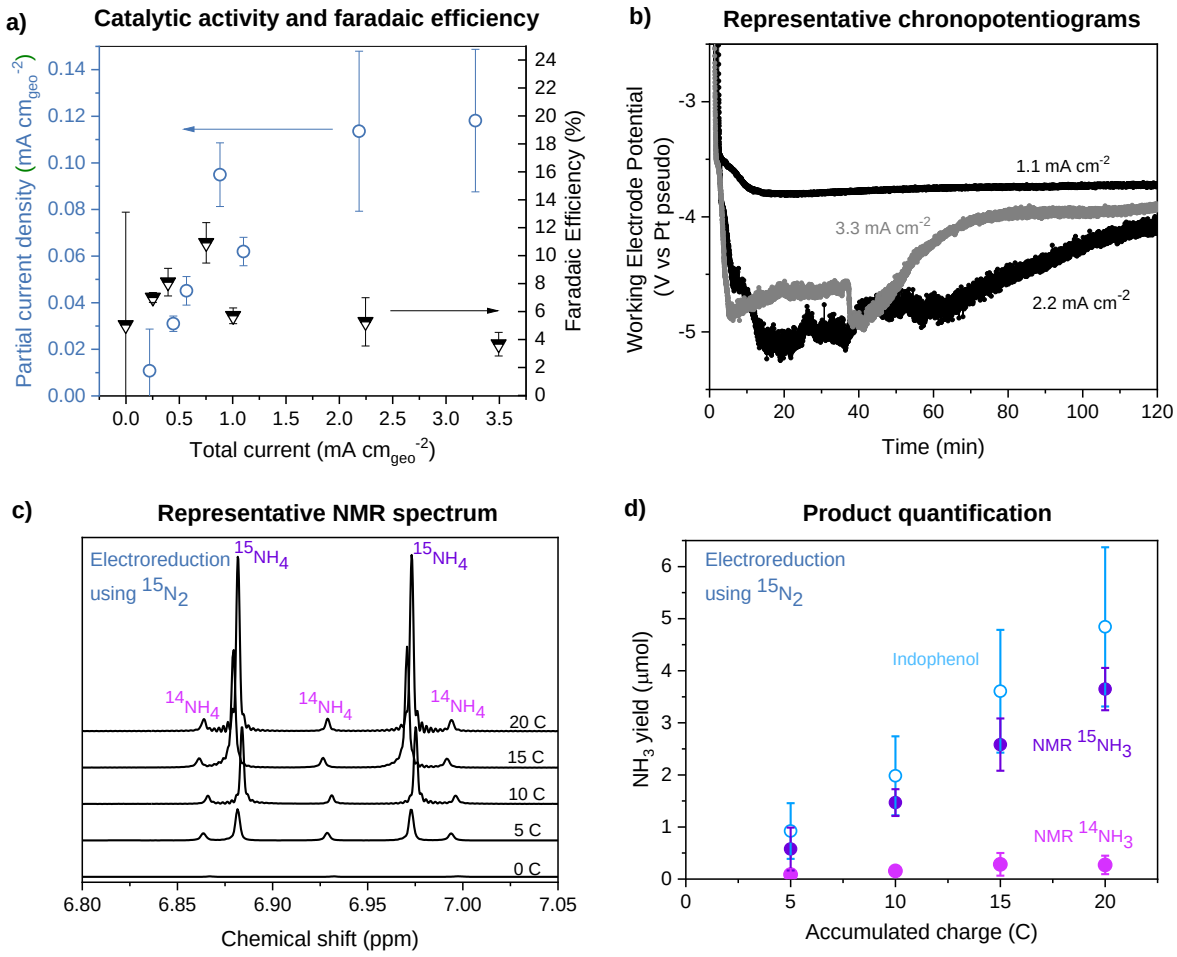

Fig. 7. Example data of Li-mediated NH_3 synthesis in THF with $LiClO_4$ salt and EtOH as the proton source. a) Partial current density to NH_3 (i_{NH3}, left y-axis) and Faradaic efficiency (FE_{NH3}, right y-axis) as a function of total applied current. b) Representative CPs for experiments plotted in panel a. c) Representative NMR data from a single measurement, with samples taken every 5 Coulumb of charge passed (C) using cleaned $^{15}N_2$ as feed-gas. d) Yield of NH_3 as a function of charge passed, showing quantitative agreement between isotope sensitive results (purple and pink) with non-isotope sensitive result (blue). Error bars signify mean and standard deviation of 3 repeated identical but independently prepared experiments. Panels a and b are reprinted with permission from REF[79], Wiley. Panels c and d are reprinted from REF[76], Springer Nature Limited.

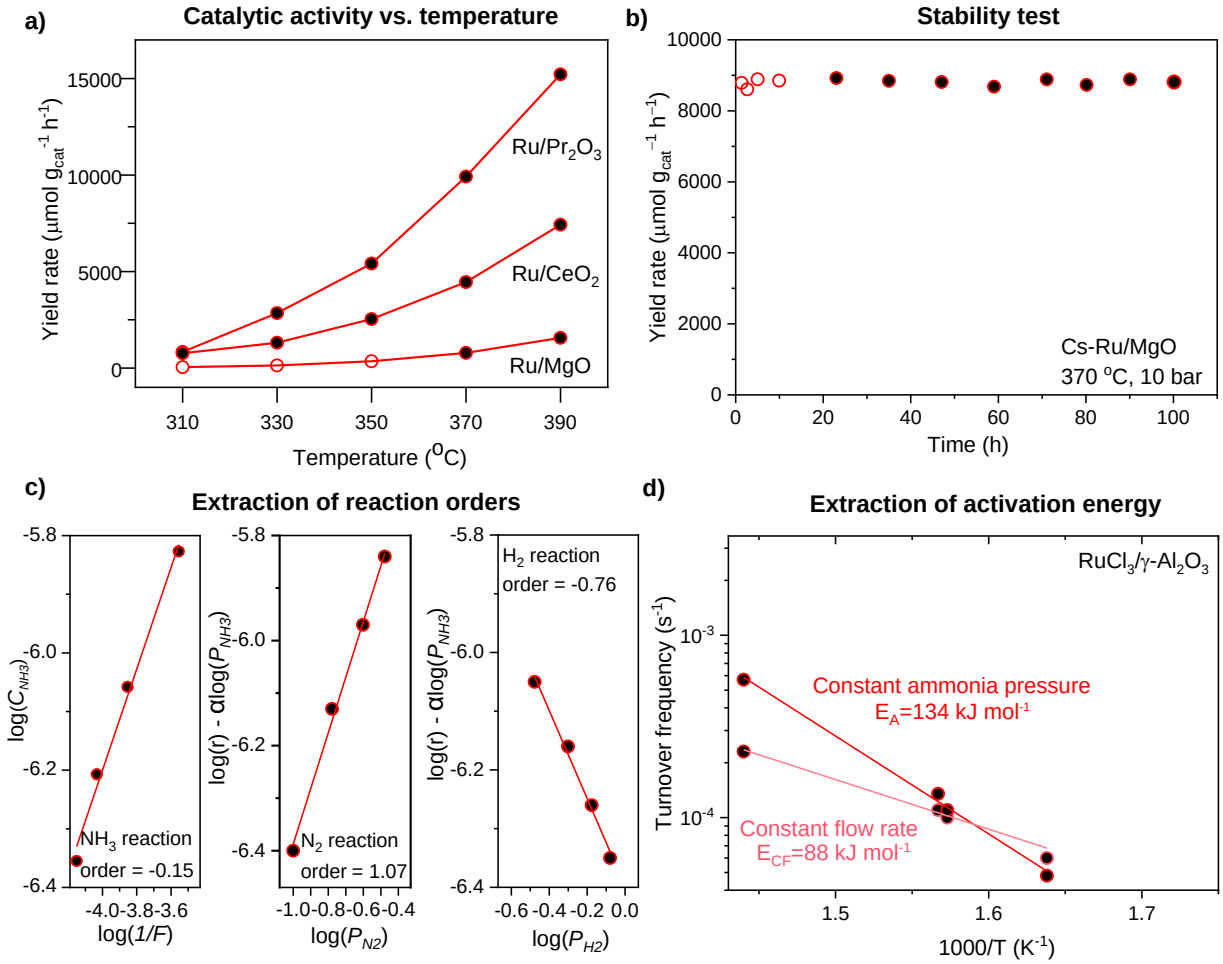

Fig. 8. Recommended reports of catalytic performances for thermal NH_3 synthesis. (a) NH_3 synthesis rate as a function of temperature[209]; (b) Stability test of NH_3 synthesis rate[114] (c) extraction of reaction orders with respect to NH_3, N_2, and H_2[221]. (d). Arrhenius plots at constant NH_3 pressure (red) and at constant flow rate (lighter red) resulting in a difference in the extracted activation energy[153]. Dark-filled points satisfy both $mass_{prod} > 2mass_{sys}$ and $C_{prod} > 100$ ppm criteria. Panel a is reprinted from REF[209], CC BY 3.0 (https://creativecommons.org/licenses/by/3.0/). Panel b is adapted with permission from Wu, S. et al. Removal of Hydrogen Poisoning by Electrostatically Polar MgO Support for Low-Pressure NH3 Synthesis at a High Rate over the Ru Catalyst. *ACS Catal.* **10**, 5614–5622 (2020). Copyright 2020 American Chemical Society. Panel c is reprinted from REF[221], CC BY 3.0 (https://creativecommons.org/licenses/by/3.0/). Panel d is reprinted with permission from REF[153], Elsevier.

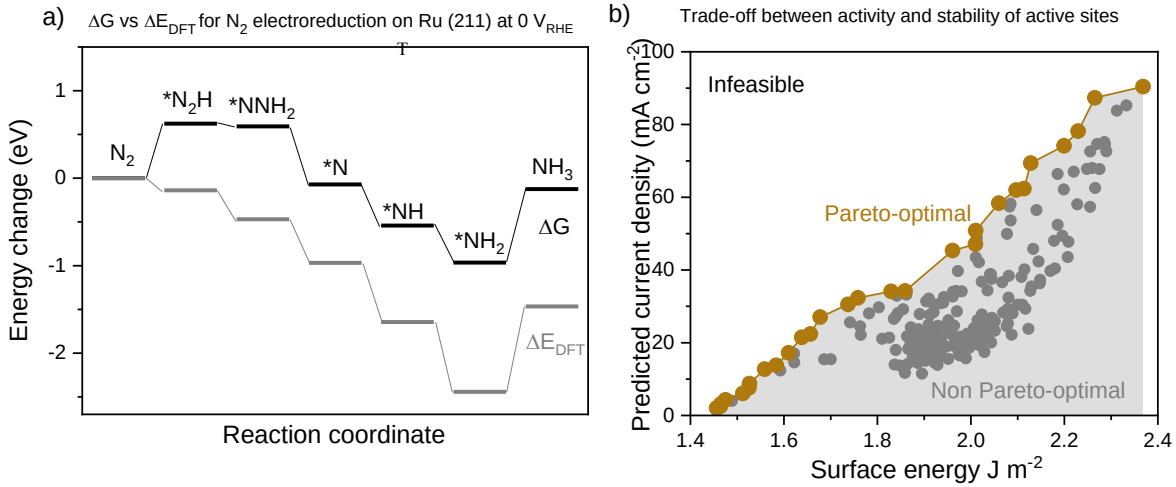

Fig. 9. **Density functional theory results.** (a) An energy diagram of N_2 reduction on Ru (211) showing the free energies and DFT energies respectively (black and grey respectively[65]). (b) The surface energy plotted against the predicted current density for the O_2 reduction reaction (ORR) on defected Pt (111) surfaces. Beige points represent points on the Pareto Frontier, grey points represent non Pareto-optimal surfaces. The grey area represents sub optimal surfaces whereas the white region represents unobtainable surfaces[166]. The current density (i) is calculated using the expression $i = i_c \exp(-\Delta G_{ORR}/kT)$, where i_c is an experimental value 3.68×10^{11} kA mol^{-1} at cell potential 0.9 V, and ΔG_{ORR} is the change in Gibbs energy of the limiting step. The surface energy of each defected surface is calculated by dividing the formation energy by the surface area. The full methodology can be found in REF[166]. In panel a, ΔG data were adopted with permission from REF[73], Royal Society of Chemistry, and the DFT energy points were acquired from J. Montoya. Panel b is reprinted from REF[166], Springer Nature Limited.

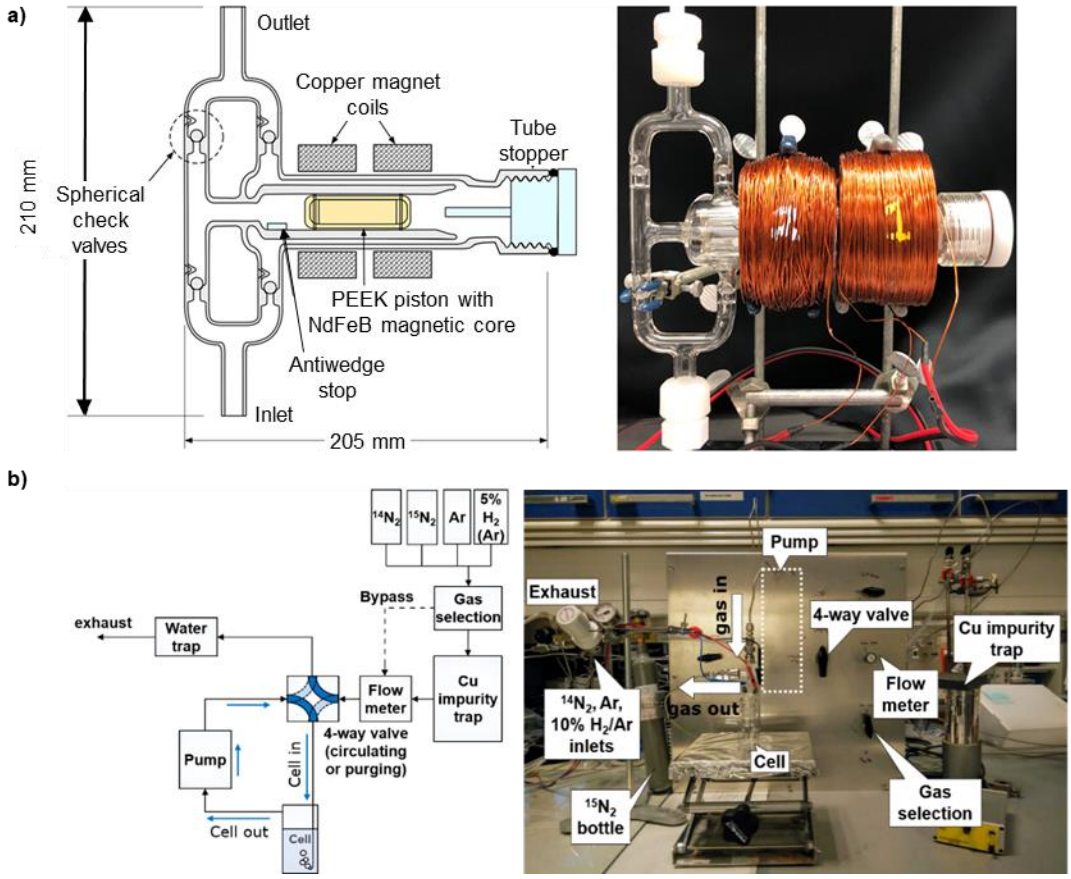

Fig. 10. Home-built glass circulation pump and full gas recirculating setup with home-built activated Cu catalyst for gas cleaning. a) Glass circulation pump, enabling long-duration experiments without supplying continuous $^{15}N_2$. b) Inexpensive gas cleaning system with a reduced Cu catalyst, freeze trap and glass circulation pump for cheap $^{15}N_2$ experimentation. Panel a is adapted with permission from REF[176] Nielander, A. C. *et al.* Readily Constructed Glass Piston Pump for Gas Recirculation. *ACS Omega* **5**, 16455–16459 (2020). Copyright 2020 American Chemical Society. Panel b is reprinted from REF[76], Springer Nature Limited.

Acknowledgment

Y.S.-H gratefully acknowledges the support by Toyota Research Institute through the Accelerated Materials Design and Discovery Program. H.I. acknowledges support from the Imperial-MIT Department of Materials Exchange Program S.Z.A. and I.C. gratefully acknowledge the funding by Villum Fonden, part of the Villum Center for the Science of Sustainable Fuels and Chemicals (V-SUSTAIN grant 9455) and Innovationsfonden (E-ammonia grant 9067-00010B). P.C. and X.L. were supported by the National Natural Science Foundation of China (Grant Nos. 21633011 and 21988101). The material based upon work by A.J.M. and B.C. was supported by the National Science Foundation under Grant No.1943707. I.E.L.S. and J.B. would like to acknowledge financial support from the Engineering and Physical Sciences Research Council (EP/M0138/1), the European Research Council (ERC) under the European Union's Horizon 2020 research and innovation programme (grant agreement No. 866402) and the National Research Council Canada through the Materials for Clean Fuels Challenge Program. We thank Marta Hatzell and Zhichuan J. Xu for the insightful discussion regarding N_2 oxidation. We thank Vahid Shadravan for helpful advice on thermochemical catalysis. We would like to acknowledge Joseph Montoya for providing data on the vibrational frequencies and free energy calculations for N_2 reduction on Ru (211) for Fig. 9a.

Competing interests

The authors declare no competing interests.

Author Contributions

Introduction (H.I., S.Z.A., and Y. S.-H.); Experimentation (S.Z.A., H.I., X.Z., J.B., P.C., I.E.L.S., I.C., and Y. S.-H.); Results (S.Z.A., H.I., X.Z., B.M.C., J.B., P.C., I.C., A.J.M., and Y. S.-H.); Applications (H.I. and S.Z.A.); Reproducibility and data deposition (H.I. and I.C.); Limitations and optimizations (S.Z.A.); Outlook (H.I., S.Z.A., J.B., X.Z. and I.E.L.S.); Overview of the Primer (H.I., S.Z.A., and Y. S.-H.). All authors discussed and edited the full manuscript.

References

1. Cottrell, T. L. The Strengths of Chemical Bonds, 2nd Ed. *Prop. atoms, radicals, Bond* (1966).

2. Jia, H.-P. & Quadrelli, E. A. Mechanistic aspects of dinitrogen cleavage and hydrogenation to produce ammonia in catalysis and organometallic chemistry: relevance of metal hydride bonds and dihydrogen. *Chem. Soc. Rev.* **43**, 547–564 (2014).

3. Noxon, J. F. Atmospheric nitrogen fixation by lightning. *Geophys. Res. Lett.* (1976).

4. Rivera Ortiz, J. M. & Burris, R. H. Interactions among substrates and inhibitors of nitrogenase. *J. Bacteriol.* (1975).

5. Yang, Z. Y. *et al.* Evidence That the Pi Release Event Is the Rate-Limiting Step in the Nitrogenase Catalytic Cycle. *Biochemistry* (2016).

6. Hoffman, B. M., Lukoyanov, D., Yang, Z., Dean, D. R. & Seefeldt, L. C. Mechanism of Nitrogen Fixation by Nitrogenase: The Next Stage. *Chem. Rev.* **114**, 4041–4062 (2014).

7. Smil, V. *Enriching the Earth: Fritz Haber, Carl Bosch, and the Transformation of World Food Production*. (The MIT Press, 2001).

8. Hager, T. *The Alchemy of Air: A Jewish Genius, a Doomed Tycoon, and the Discovery that Changed the Course of History*. *Broadway Books* (Broadway Books, 2008).

9. Science and Food Supplies. *Nature* **126**, 193–194 (1930).

10. Ihde, A. J. *The Development of Modern Chemistry (Dover Books on Chemistry)*. (Dover Publications, 1984).

11. Chen, J. G. *et al.* Beyond fossil fuel–driven nitrogen transformations. *Science (80-.).* **360**, eaar6611 (2018).

    This review covers the thermochemistry of all nitrogen transformation reactions, and the challenges and opportunities associated with these reactions in overcoming reliance on fossil fuels.

12. Smith, C., Hill, A. K. & Torrente-Murciano, L. Current and future role of Haber–Bosch ammonia in a carbon-free energy landscape. *Energy Environ. Sci.* (2020).

13. Aika, K. & Tamara, K. Ammonia Synthesis over Non-Iron Catalysts and Related Phenomena. in *Ammonia* (1995).

14. Ertl, G. Reactions at Surfaces: From Atoms to Complexity (Nobel Lecture). *Angew. Chemie Int. Ed.* **47**, 3524–3535 (2008).

15. Erisman, J. W., Sutton, M. a., Galloway, J., Klimont, Z. & Winiwarter, W. How a century of ammonia synthesis changed the world. *Nat. Geosci.* **1**, 636–639 (2008).

16. Smil, V. Nitrogen and Food Production: Proteins for Human Diets. *AMBIO A J. Hum. Environ.* **31**, 126–131 (2002).

17. Stewart, W. M., Dibb, D. W., Johnston, A. E. & Smyth, T. J. The Contribution of Commercial Fertilizer Nutrients to Food Production. *Agron. J.* **97**, 1–6 (2005).

18. USGS National Minerals Information Center. *Nitrogen Statistics and Information, U.S. Geological Survey, Mineral Commodity Summaries, January 2020*. (2020).

19. Apodaca, L. E. Nitrogen (fixed) — Ammonia. 116–117 (2021).

https://www.usgs.gov/centers/nmic/nitrogen-statistics-and-information

20. Smil, V. Detonator of the population explosion. *Nature* **400**, 415–415 (1999).

21. Schlögl, R. Ammonia Synthesis. in *Handbook of Heterogeneous Catalysis* 2501 (Wiley-VCH Verlag GmbH & Co. KGaA, 2008).

22. IHS Markit. *Ammonia - Chemical Economics Handbook (CEH) | IHS Markit*. *IHSmarkit.com* (2020).

23. Klerke, A., Christensen, C. H., Nørskov, J. K. & Vegge, T. Ammonia for hydrogen storage: challenges and opportunities. *J. Mater. Chem.* **18**, 2304 (2008).

24. Zamfirescu, C. & Dincer, I. Using ammonia as a sustainable fuel. *J. Power Sources* **185**, 459–465 (2008).

25. Brightling, J. Ammonia and the Fertiliser Industry: The Development of Ammonia at Billingham A history of technological innovation from the early 20th century to the present day. *Johnson Matthey Technol. Rev.* (2018).

26. Brown, T. Ammonia production causes 1% of total global GHG emissions. Ammoniaindustry. https://ammoniaindustry.com/ammonia-production-causes-1-percent-of-total-global-ghg-emissions/

27. Soloveichik, G. Electrochemical synthesis of ammonia as a potential alternative to the Haber–Bosch process. *Nature Catalysis* (2019) doi:10.1038/s41929-019-0280-0.

28. MacFarlane, D. R. *et al.* A Roadmap to the Ammonia Economy. *Joule* **4**, 1186–1205 (2020).

This paper covers 3 different generations of technological advancement needed to produce ammonia sustainably.

29. Stephens, I. & Nilsson, A. Research needs towards sustainable production of fuels and chemicals. *Energy-X, Chapter 5* (2019). https://www.energy-x.eu/research-needs-report/

30. Erisman, J. W., Bleeker, A., Galloway, J. & Sutton, M. S. Reduced nitrogen in ecology and the environment. *Environ. Pollut.* **150**, 140–149 (2007).

31. Good, A. G. & Beatty, P. H. Fertilizing nature: A tragedy of excess in the commons. *PLoS Biol.* **9**, 1–9 (2011).

32. Singh, A. R. *et al.* Electrochemical Ammonia Synthesis - The Selectivity Challenge. *ACS Catal.* **7**, 706–709 (2017).

This viewpoint illucidates the selectivity challenge by covering a qualitative analysis of electrochemical ammonia synthesis and suggests strategies to circumvent the issue.

33. Comer, B. M. *et al.* Prospects and Challenges for Solar Fertilizers. *Joule* (2019).

34. Ummary, S. Renewable Energy to Fuels Through Utilization of EnergyDense Liquids (REFUEL) Program Overview. 1–16 (2016). https://arpa-e.energy.gov/sites/default/files/documents/files/REFUEL_ProgramOverview.pdf

35. Rouwenhorst, K. H. R., Kim, H. H. & Lefferts, L. Vibrationally Excited Activation of N2 in Plasma-Enhanced Catalytic Ammonia Synthesis: A Kinetic Analysis. *ACS Sustain. Chem. Eng.* (2019).

36. Rouwenhorst, K. H. R. *et al.* Plasma-driven catalysis: Green ammonia synthesis with intermittent electricity. *Green Chem.* (2020) doi:10.1039/d0gc02058c.

37. Kim, H. H., Teramoto, Y., Ogata, A., Takagi, H. & Nanba, T. Atmospheric-pressure nonthermal plasma synthesis of ammonia over ruthenium catalysts. *Plasma Process. Polym.* (2017) doi:10.1002/ppap.201600157.

38. Mehta, P. *et al.* Overcoming ammonia synthesis scaling relations with plasma-enabled catalysis. *Nat. Catal.* (2018).

39. Han, G.-F. *et al.* Mechanochemistry for ammonia synthesis under mild conditions. *Nat. Nanotechnol.* (2020).

40. Tricker, A. W. *et al.* Mechanocatalytic Ammonia Synthesis over TiN in Transient Microenvironments. *ACS Energy Lett.* **5**, 3362–3367 (2020).

41. IHS. *Nitric acid - Chemical Economics Handbooks (CEH)* | IHS Markit. IHSmarkit.com (2015).

42. Bard, a & Faulkner, L. Chapter 2, Electrochemical Methods: Fundamentals and Applications, New York: , 2001. *Russ. J. Electrochem.* (2002).

43. Patil, B. S., Rovira Palau, J., Hessel, V., Lang, J. & Wang, Q. Plasma Nitrogen Oxides Synthesis in a Milli-Scale Gliding Arc Reactor: Investigating the Electrical and Process Parameters. *Plasma Chem. Plasma Process.* **36**, 241–257 (2016).

44. Birkeland, K. R. On the oxidation of atmospheric nitrogen in electric arcs. *Trans. Faraday Soc.* (1906).

45. Eyde, S. Oxidation of atmospheric nitrogen and development of resulting industries in norway. *Ind. Eng. Chem.* (1912).

46. Cherkasov, N., Ibhadon, A. O. & Fitzpatrick, P. A review of the existing and alternative methods for greener nitrogen fixation. *Chemical Engineering and Processing: Process Intensification* (2015).

47. Hessel, V. *et al.* Industrial applications of plasma, microwave and ultrasound techniques: Nitrogen-fixation and hydrogenation reactions. *Chem. Eng. Process. Process Intensif.* (2013).

48. Rusanov, V. D., Fridman, A. A. & Sholin, G. V. The Physics of a Chemically Active Plasma With Nonequilibrium Vibrational Excitationc of Molecules. *Sov. Phys. - Uspekhi* (1981).

49. Li, S., Medrano, J. A., Hessel, V. & Gallucci, F. Recent progress of plasma-assisted nitrogen fixation research: A review. *Processes* (2018).

50. Dai, C., Sun, Y., Chen, G., Fisher, A. C. & Xu, Z. J. Electrochemical Oxidation of Nitrogen towards Direct Nitrate Production on Spinel Oxides. *Angew. Chemie Int. Ed.* **59**, 9418–9422 (2020).

51. Fang, W. *et al.* Boosting efficient ambient nitrogen oxidation by a well-dispersed Pd on MXene electrocatalyst. *Chem. Commun.* **56**, 5779–5782 (2020).

52. Wang, Y., Yu, Y., Jia, R., Zhang, C. & Zhang, B. Electrochemical synthesis of nitric acid from air and ammonia through waste utilization. *Natl. Sci. Rev.* **6**, 730–738 (2019).

53. Lun Pang, C., Lindsay, R. & Thornton, G. Chemical reactions on rutile TiO2(110). *Chem. Soc. Rev.* (2008).

54. Bickley, R. I. & Vishwanathan, V. Photocatalytically induced fixation of molecular nitrogen by near UV radiation [6]. *Nature* (1979).

55. Yuan, S. J. *et al.* Nitrate formation from atmospheric nitrogen and oxygen photocatalysed by nano-sized titanium dioxide. *Nat. Commun.* (2013).

56. Kuang, M. *et al.* Efficient Nitrate Synthesis via Ambient Nitrogen Oxidation with Ru-Doped TiO 2 /RuO 2 Electrocatalysts. *Adv. Mater.* **32**, 2002189 (2020).

57. Wang, S. *et al.* Universal transition state scaling relations for (de)hydrogenation over transition metals. *Phys. Chem. Chem. Phys.* (2011).

58. Bozso, F., Ertl, G., Grunze, M. & Weiss, M. Interaction of nitrogen with iron surfaces. I. Fe(100) and Fe(111). *J. Catal.* (1977).

59. Bozso, F., Ertl, G. & Weiss, M. Interaction of nitrogen with iron surfaces. II. Fe(110). *J. Catal.* (1977).

60. Ertl, G., Lee, S. B. & Weiss, M. Adsorption of nitrogen on potassium promoted Fe(111) and (100) surfaces. *Surf. Sci.* (1982).

61. Honkala, K. *et al.* Ammonia synthesis from first-principles calculations. *Science (80-.).* (2005).

62. Dahl, S. *et al.* Role of steps in N2 activation on Ru(0001). *Phys. Rev. Lett.* (1999).

63. Chorkendorff, I. & Niemantsverdriet, J. W. Chapter 3: Reaction Rate Theory. in *Concepts of Modern Catalysis and Kinetics* (John Wiley and Sons, 2003).

64. Medford, A. J. & Hatzell, M. C. Photon-Driven Nitrogen Fixation: Current Progress, Thermodynamic Considerations, and Future Outlook. *ACS Catal.* **7**, 2624–2643 (2017).

65. Comer, B. M. & Medford, A. J. Analysis of Photocatalytic Nitrogen Fixation on Rutile TiO2(110). *ACS Sustain. Chem. Eng.* **6**, 4648–4660 (2018).

66. Singh, A. R. *et al.* Strategies toward Selective Electrochemical Ammonia Synthesis. *ACS Catal.* **9**, 8316–8324 (2019).

67. Medford, A. J. *et al.* Assessing the reliability of calculated catalytic ammonia synthesis rates. *Science (80-.).* (2014).

68. Wellendorff, J. *et al.* Density functionals for surface science: Exchange-correlation model development with Bayesian error estimation. *Phys. Rev. B - Condens. Matter Mater. Phys.* (2012).

69. Medford, A. J. *et al.* From the Sabatier principle to a predictive theory of transition-metal heterogeneous catalysis. *J. Catal.* **328**, 36–42 (2015).

This paper discusses scaling relations, activity maps, and the d-band model, thereby mapping out the development of trends in transisiton-matal catalysts.

70. Bare, S. R., Strongin, D. R. & Somorjai, G. A. Ammonia synthesis over iron single-crystal catalysts: The effects of alumina and potassium. *J. Phys. Chem.* (1986).

71. Dahl, S., Taylor, P. A., Törnqvist, E. & Chorkendorff, I. The synthesis of ammonia over a ruthenium single crystal. *J. Catal.* (1998).

72. Singh, A. R. *et al.* Computational Design of Active Site Structures with Improved Transition-State Scaling for Ammonia Synthesis. *ACS Catal.* (2018).

73. Montoya, J. H., Tsai, C., Vojvodic, A. & Nørskov, J. K. The Challenge of Electrochemical Ammonia Synthesis: A New Perspective on the Role of Nitrogen Scaling Relations. *ChemSusChem* **8**, 2180–2186 (2015).

This paper presents insights from DFT calculations that describe limitations on the low-temperature electrocatalytic production of ammonia from dinitrogen.

74. Skúlason, E. *et al.* A theoretical evaluation of possible transition metal electro-catalysts for N2 reduction. *Phys. Chem. Chem. Phys.* **14**, 1235–1245 (2012).

75. Rostamikia, G., Maheshwari, S. & Janik, M. J. Elementary kinetics of nitrogen electroreduction to ammonia on late transition metals. *Catal. Sci. Technol.* (2019).

76. Andersen, S. Z. *et al.* A rigorous electrochemical ammonia synthesis protocol with quantitative isotope measurements. *Nature* **570**, 504–508 (2019).

This letter provides a rigorous protocol from which the source of activated nitrogen can be determined.

77. Suryanto, B. H. R. *et al.* Challenges and prospects in the catalysis of electroreduction of nitrogen to ammonia. *Nat. Catal.* **2**, 290–296 (2019).

78. Wang, P. *et al.* Breaking scaling relations to achieve low-temperature ammonia synthesis through LiH-mediated nitrogen transfer and hydrogenation. *Nat. Chem.* **9**, 64–70 (2017).

This study designed a two-active-center strategy using TM(N)-LiH composite catalysts to create an energy-efficient pathway that allows NH_3 synthesis under mild conditions.

79. Schwalbe, J. A. *et al.* A Combined Theory-Experiment Analysis of the Surface Species in Lithium-Mediated NH3 Electrosynthesis. *ChemElectroChem* **7**, 1542–1549 (2020).

80. Lazouski, N., Chung, M., Williams, K., Gala, M. L. & Manthiram, K. Non-aqueous gas diffusion electrodes for rapid ammonia synthesis from nitrogen and water-splitting-derived hydrogen. *Nat. Catal.* **3**, 463–469 (2020).

81. Lazouski, N., Schiffer, Z. J., Williams, K. & Manthiram, K. Understanding Continuous Lithium-Mediated Electrochemical Nitrogen Reduction. *Joule* **3**, 1127–1139 (2019).

82. Andersen, S. Z. *et al.* Increasing stability, efficiency, and fundamental understanding of lithium-mediated electrochemical nitrogen reduction. *Energy Environ. Sci.* **13**, 4291–4300 (2020).

83. McEnaney, J. M. *et al.* Ammonia synthesis from N2 and H2O using a lithium cycling electrification strategy at atmospheric pressure. *Energy Environ. Sci.* **10**, 1621–1630 (2017).

84. Kim, K. *et al.* Lithium-Mediated Ammonia Electro-Synthesis: Effect of CsClO 4 on Lithium Plating Efficiency and Ammonia Synthesis . *J. Electrochem. Soc.* (2018).

85. Hattori, M., Iijima, S., Nakao, T., Hosono, H. & Hara, M. Solid solution for catalytic ammonia synthesis from nitrogen and hydrogen gases at 50 °C. *Nat. Commun.* **11**, 2001 (2020).

86. Davy, H. The Bakerian Lecture, on some chemical agencies of electricity. *Philos. Trans. R. Soc. London* **97**, 1–56 (1807).

87. Rayleigh, Lord. XIII.—Observations on the oxidation of nitrogen gas. *J. Chem. Soc., Trans.* **71**, 181–186 (1897).

88. Boucher, D. L., Davies, J. A., Edwards, J. G. & Mennad, A. An investigation of the putative photosynthesis of ammonia on iron-doped titania and other metal oxides. *J. Photochem. Photobiol. A Chem.* **88**, 53–64 (1995).

89. Shipman, M. A. & Symes, M. D. A re-evaluation of Sn(II) phthalocyanine as a catalyst for the electrosynthesis of ammonia. *Electrochim. Acta* **258**, 618–622 (2017).

90. Licht, S. *et al.* Retraction. *Science (80-.).* **369**, 780 (2020).

91. Du, H.-L., Gengenbach, T. R., Hodgetts, R., MacFarlane, D. R. & Simonov, A. N. Critical

Assessment of the Electrocatalytic Activity of Vanadium and Niobium Nitrides toward Dinitrogen Reduction to Ammonia. *ACS Sustain. Chem. Eng.* **7**, 6839–6850 (2019).

92. Choi, J. *et al.* Promoting nitrogen electroreduction to ammonia with bismuth nanocrystals and potassium cations in water. *ChemRxiv, Prepr.* (2020).

93. Yang, X. *et al.* Quantification of Active Sites and Elucidation of the Reaction Mechanism of the Electrochemical Nitrogen Reduction Reaction on Vanadium Nitride. *Angew. Chemie* **131**, 13906–13910 (2019).

94. Bao, D. *et al.* Electrochemical Reduction of N2 under Ambient Conditions for Artificial N2 Fixation and Renewable Energy Storage Using N2/NH3 Cycle. *Adv. Mater.* **29**, 1604799 (2017).

95. Hao, Y.-C. *et al.* Promoting nitrogen electroreduction to ammonia with bismuth nanocrystals and potassium cations in water. *Nat. Catal.* **2**, 448–456 (2019).

96. Smeets, M. A. M. *et al.* Odor and Irritation Thresholds for Ammonia: A Comparison between Static and Dynamic Olfactometry. *Chem. Senses* **32**, 11–20 (2007).

97. Dabundo, R. *et al.* The Contamination of Commercial 15N2 Gas Stocks with 15N–Labeled Nitrate and Ammonium and Consequences for Nitrogen Fixation Measurements. *PLoS One* **9**, e110335 (2014).

This paper shows that commercial isotope labelled $^{15}N_2$ contains significant contamination across lot numbers and different manufacturers.

98. Giordano, L. *et al.* PH dependence of OER activity of oxides: Current and future perspectives. *Catal. Today* **262**, 2–10 (2016).

99. Shinagawa, T., Garcia-Esparza, A. T. & Takanabe, K. Insight on Tafel slopes from a microkinetic analysis of aqueous electrocatalysis for energy conversion. *Sci. Rep.* **5**, 13801 (2015).

100. Limaye, A., Zeng, J. S., Willard, A. & Manthiram, K. Bayesian Data Analysis Reveals No Preference for Cardinal Tafel Slopes in CO2 Reduction Electrocatalysis. *ChemRxiv* (2020).

101. Neyerlin, K. C., Gu, W., Jorne, J. & Gasteiger, H. A. Determination of Catalyst Unique Parameters for the Oxygen Reduction Reaction in a PEMFC. *J. Electrochem. Soc.* **153**, A1955 (2006).

102. Choi, J. *et al.* Identification and elimination of false positives in electrochemical nitrogen reduction studies. *Nat. Commun.* **11**, 5546 (2020).

This perspective assesses a wide range of electrocatalytic nitrogen reduction reports identifying false positives and providing an experimental protocol for ensuring rigorous ammonia quantification in upcoming works.

103. Wei, C. *et al.* Recommended Practices and Benchmark Activity for Hydrogen and Oxygen Electrocatalysis in Water Splitting and Fuel Cells. *Adv. Mater.* **31**, 1806296 (2019).

104. Ledezma-Yanez, I., Díaz-Morales, O., Figueiredo, M. C. & Koper, M. T. M. Hydrogen Oxidation and Hydrogen Evolution on a Platinum Electrode in Acetonitrile. *ChemElectroChem* **2**, 1612–1622 (2015).

105. Raccichini, R., Amores, M. & Hinds, G. Critical review of the use of reference electrodes in li-ion batteries: A diagnostic perspective. *Batteries* (2019) doi:10.3390/batteries5010012.

106. Ren, Y. *et al.* Is It Appropriate to Use the Nafion Membrane in Electrocatalytic N2 Reduction? *Small Methods* **3**, 1900474 (2019).

107. Liu, H., Zhang, Y. & Luo, J. The removal of inevitable NO species in catalysts and the selection of appropriate membrane for measuring electrocatalytic ammonia synthesis accurately. *J. Energy Chem.* **49**, 51–58 (2020).

108. Hongsirikarn, K., Goodwin, J. G., Greenway, S. & Creager, S. Influence of ammonia on the conductivity of Nafion membranes. *J. Power Sources* **195**, 30–38 (2010).

109. Halseid, R., Vie, P. J. S. & Tunold, R. Influence of Ammonium on Conductivity and Water Content of Nafion 117 Membranes. *J. Electrochem. Soc.* **151**, A381 (2004).

110. Lindley, B. M., Appel, A. M., Krogh-Jespersen, K., Mayer, J. M. & Miller, A. J. M. Evaluating the Thermodynamics of Electrocatalytic N 2 Reduction in Acetonitrile. *ACS Energy Lett.* **1**, 698–704 (2016).

111. Guo, J. *et al.* Lithium imide synergy with 3d transition-metal nitrides leading to unprecedented catalytic activities for ammonia decomposition. *Angew. Chemie, Int. Ed. English* **54**, 2950–2954 (2015).

112. Kitano, M. *et al.* Ammonia synthesis using a stable electride as an electron donor and reversible hydrogen store. *Nat. Chem.* **4**, 934–940 (2012).

113. Ma, Z., Zhao, S., Pei, X., Xiong, X. & Hu, B. New insights into the support morphology-dependent ammonia synthesis activity of Ru/CeO2 catalysts. *Catal. Sci. Technol.* **7**, 191–199 (2017).

114. Wu, S. *et al.* Removal of Hydrogen Poisoning by Electrostatically Polar MgO Support for Low-Pressure NH3 Synthesis at a High Rate over the Ru Catalyst. *ACS Catal.* **10**, 5614–5622 (2020).

115. Searle, P. L. The berthelot or indophenol reaction and its use in the analytical chemistry of nitrogen. A review. *Analyst* **109**, 549 (1984).

116. Zhao, Y. *et al.* Ammonia Detection Methods in Photocatalytic and Electrocatalytic Experiments: How to Improve the Reliability of NH 3 Production Rates? *Adv. Sci.* **6**, (2019).

117. Zhou, L. & Boyd, C. E. Comparison of Nessler, phenate, salicylate and ion selective electrode procedures for determination of total ammonia nitrogen in aquaculture. *Aquaculture* **450**, 187–193 (2016).

118. Giner-Sanz, J. J., Leverick, G. M., Pérez-Herranz, V. & Shao-Horn, Y. Salicylate Method for Ammonia Quantification in Nitrogen Electroreduction Experiments: The Correction of Iron III Interference. *J. Electrochem. Soc.* **167**, 134519 (2020).

119. Murray, E. *et al.* A colorimetric method for use within portable test kits for nitrate determination in various water matrices. *Anal. Methods* **9**, 680–687 (2017).

120. Hayashi, M. Temperature-electrical conductivity relation of water for environmental monitoring and geophysical data inversion. *Environ. Monit. Assess.* **96**, 119–128 (2004).

121. Bruker. What Is NMR? *Bruker BioSpin* 145–158 (2010).

122. Nielander, A. C. *et al.* A Versatile Method for Ammonia Detection in a Range of Relevant Electrolytes via Direct Nuclear Magnetic Resonance Techniques. *ACS Catal.* **9**, 5797–5802 (2019).

This paper reports on a frequency-selective pulse nuclear magnetic resonance method for the accurate determination of ammonia.

123. Mooney, E. F. & Winson, P. H. Nitrogen Magnetic Resonance Spectroscopy. *Annu. Reports NMR*

Spectrosc. **2**, 125–152 (1969).

124. Giddey, S., Badwal, S. P. S. & Kulkarni, A. Review of electrochemical ammonia production technologies and materials. *Int. J. Hydrogen Energy* **38**, 14576–14594 (2013).

125. Seh, Z. W. *et al.* Combining theory and experiment in electrocatalysis: Insights into materials design. *Science (80-.).* **355**, eaad4998 (2017).

126. Choi, J. *et al.* Electroreduction of Nitrates, Nitrites, and Gaseous Nitrogen Oxides: A Potential Source of Ammonia in Dinitrogen Reduction Studies. *ACS Energy Lett.* **5**, 2095–2097 (2020).

127. Li, J. & Wu, N. Semiconductor-based photocatalysts and photoelectrochemical cells for solar fuel generation: A review. *Catalysis Science and Technology* (2015).

128. Kisch, H. Semiconductor Photocatalysis-Mechanistic and Synthetic Aspects. *Angew. Chemie Int. Ed.* **52**, 812–847 (2013).

129. Chen, X., Shen, S., Guo, L. & Mao, S. S. Semiconductor-based Photocatalytic Hydrogen Generation. *Chem. Rev.* **110**, 6503–6570 (2010).

130. Kibsgaard, J., Nørskov, J. K. & Chorkendorff, I. The Difficulty of Proving Electrochemical Ammonia Synthesis. *ACS Energy Lett.* **4**, 2986–2988 (2019).

131. Turner, C., Španěl, P. & Smith, D. A longitudinal study of ammonia, acetone and propanol in the exhaled breath of 30 subjects using selected ion flow tube mass spectrometry, SIFT-MS. *Physiol. Meas.* **27**, 321–337 (2006).

132. Tao, H. *et al.* Nitrogen Fixation by Ru Single-Atom Electrocatalytic Reduction. *Chem* **5**, 204–214 (2019).

133. Xiong, W. *et al.* Facile, cost-effective plasma synthesis of self-supportive FeS x on Fe foam for efficient electrochemical reduction of N 2 under ambient conditions. *J. Mater. Chem. A* **7**, 19977–19983 (2019).

134. Suryanto, B. H. R. *et al.* MoS 2 Polymorphic Engineering Enhances Selectivity in the Electrochemical Reduction of Nitrogen to Ammonia. *ACS Energy Lett.* **4**, 430–435 (2019).

135. Li, X. *et al.* Boosted Electrocatalytic N2 Reduction to NH3 by Defect-Rich MoS2 Nanoflower. *Adv. Energy Mater.* **8**, (2018).

136. Chen, G.-F. *et al.* Ammonia Electrosynthesis with High Selectivity under Ambient Conditions via a Li+ Incorporation Strategy. *J. Am. Chem. Soc.* **139**, 9771–9774 (2017).

137. Song, Y. *et al.* A physical catalyst for the electrolysis of nitrogen to ammonia. *Sci. Adv.* **4**, e1700336 (2018).

138. Zhou, F. *et al.* Electro-synthesis of ammonia from nitrogen at ambient temperature and pressure in ionic liquids. *Energy Environ. Sci.* **10**, 2516–2520 (2017).

139. Tsuneto, A., Kudo, A. & Sakata, T. Lithium-mediated electrochemical reduction of high pressure N2 to NH3. *J. Electroanal. Chem.* **367**, 183–188 (1994).

140. Tsuneto, A., Kudo, A. & Sakata, T. Efficient Electrochemical Reduction of N2 to NH3 Catalyzed by Lithium. *Chem. Lett.* **22**, 851–854 (1993).

141. Zhang, L. *et al.* A Janus Fe-SnO 2 Catalyst that Enables Bifunctional Electrochemical Nitrogen Fixation. *Angew. Chemie Int. Ed.* **59**, 10888–10893 (2020).

142. Hirakawa, H., Hashimoto, M., Shiraishi, Y. & Hirai, T. Photocatalytic Conversion of Nitrogen to

Ammonia with Water on Surface Oxygen Vacancies of Titanium Dioxide. *J. Am. Chem. Soc.* **139**, 10929–10936 (2017).

143. Comer, B. M. *et al.* The Role of Adventitious Carbon in Photo-catalytic Nitrogen Fixation by Titania. *J. Am. Chem. Soc.* (2018).

144. Wang, Z. *et al.* Recent Developments in Polymeric Carbon Nitride-Derived Photocatalysts and Electrocatalysts for Nitrogen Fixation. *ACS Catalysis* (2019).

145. Lv, C. *et al.* Defect Engineering Metal-Free Polymeric Carbon Nitride Electrocatalyst for Effective Nitrogen Fixation under Ambient Conditions. *Angew. Chemie - Int. Ed.* (2018).

146. Hu, B., Hu, M., Seefeldt, L. & Liu, T. L. Electrochemical Dinitrogen Reduction to Ammonia by Mo2N: Catalysis or Decomposition? *ACS Energy Lett.* **4**, 1053–1054 (2019).

147. Liu, Q. *et al.* Photocatalytic N2 reduction: Uncertainties in the determination of ammonia production. *ACS Sustain. Chem. Eng.* (2021).

148. Bielawa, H., Hinrichsen, O., Birkner, A. & Muhler, M. The ammonia-synthesis catalyst of the next generation: Barium-promoted oxide-supported ruthenium. *Angew. Chemie-International Ed.* **40**, 1061- (2001).

149. Hagen, S. *et al.* New efficient catalyst for ammonia synthesis: barium-promoted cobalt on carbon. *Chem. Commun.* **11**, 1206–1207 (2002).

150. Kojima, R. & Aika, K. Cobalt molybdenum bimetallic nitride catalysts for ammonia synthesis Part 2. Kinetic study.pdf. *Appl. Catal. A Gen.* **218**, 121–128 (2001).

This article presents a typical kinetic study for thermocatalytic ammonia synthesis, including the measurement conditions, derivation process of the equations, and the calculations.

151. Hagen, S. Ammonia synthesis with barium-promoted iron–cobalt alloys supported on carbon. *J. Catal.* **214**, 327–335 (2003).

152. Aika, K. Role of alkali promoter in ammonia synthesis over ruthenium catalysts—Effect on reaction mechanism. *Catal. Today* **286**, 14–20 (2017).

153. Holzman, P. R., Shiflett, W. K. & Dumesic, J. A. The importance of ammonia pressure in the kinetics of ammonia synthesis over supported Ru. *J. Catal.* **62**, 167–172 (1980).

This study compared the results of apparent activation energies measured at constant ammonia pressure and at constant flow rate, demonstrating the importance of ammonia partial pressure for reaction kinetics.

154. Ye, T.-N. *et al.* Vacancy-enabled N2 activation for ammonia synthesis on an Ni-loaded catalyst. *Nature* **583**, 391–395 (2020).

155. Tang, Y. *et al.* Metal-Dependent Support Effects of Oxyhydride-Supported Ru, Fe, Co Catalysts for Ammonia Synthesis. *Adv. Energy Mater.* **8**, (2018).

156. Kobayashi, Y. *et al.* Titanium-Based Hydrides as Heterogeneous Catalysts for Ammonia Synthesis. *J. Am. Chem. Soc.* (2017).

157. Cao, Y. *et al.* Vanadium Hydride as an Ammonia Synthesis Catalyst. *ChemCatChem* (2020).

158. Kammert, J. *et al.* Nature of Reactive Hydrogen for Ammonia Synthesis over a Ru/C12A7 Electride Catalyst. *J. Am. Chem. Soc.* **142**, 7655–7667 (2020).

159. Gao, W., Guo, J. & Chen, P. Hydrides, Amides and Imides Mediated Ammonia Synthesis and

Decomposition. *Chinese J. Chem.* **37**, 442–451 (2019).

160. Peterson, A. A., Abild-Pedersen, F., Studt, F., Rossmeisl, J. & Nørskov, J. K. How copper catalyzes the electroreduction of carbon dioxide into hydrocarbon fuels. *Energy Environ. Sci.* (2010).

161. Sundararaman, R., Goddard, W. A. & Arias, T. A. Grand canonical electronic density-functional theory: Algorithms and applications to electrochemistry. *J. Chem. Phys.* (2017).

162. Kastlunger, G., Lindgren, P. & Peterson, A. A. Controlled-Potential Simulation of Elementary Electrochemical Reactions: Proton Discharge on Metal Surfaces. *J. Phys. Chem. C* (2018).

163. Govender, A., Curulla Ferré, D. & Niemantsverdriet, J. W. A density functional theory study on the effect of zero-point energy corrections on the methanation profile on Fe(100). *ChemPhysChem* (2012).

164. Sholl, D. S. & Steckel, J. A. *Density Functional Theory: A Practical Introduction, Chapter 5, Pg. 113-130*. *Density Functional Theory: A Practical Introduction* (2009).

Book chapter covering zero point energy and entropy/enthalpy energy terms, and provides a good overview of the theory.

165. Sprowl, L. H., Campbell, C. T. & Árnadóttir, L. Hindered translator and hindered rotor models for adsorbates: Partition functions and entropies. *J. Phys. Chem. C* (2016).

166. Núñez, M., Lansford, J. L. & Vlachos, D. G. Optimization of the facet structure of transition-metal catalysts applied to the oxygen reduction reaction. *Nat. Chem.* **11**, 449–456 (2019).

This paper shows trade-offs between activity and stability.

167. Goldsmith, B. R., Sanderson, E. D., Bean, D. & Peters, B. Isolated catalyst sites on amorphous supports: A systematic algorithm for understanding heterogeneities in structure and reactivity. *J. Chem. Phys.* (2013).

168. Wexler, R. B., Qiu, T. & Rappe, A. M. Automatic Prediction of Surface Phase Diagrams Using Ab Initio Grand Canonical Monte Carlo. *J. Phys. Chem. C* (2019) doi:10.1021/acs.jpcc.8b11093.

169. Shimanouchi, T. 'Molecular Vibrational Frequencies' in NIST Chemistry WebBook. *NIST Standard Reference Database Number 69*.

170. Makepeace, J. W. *et al.* Reversible ammonia-based and liquid organic hydrogen carriers for high-density hydrogen storage: Recent progress. *Int. J. Hydrogen Energy* **44**, 7746–7767 (2019).

171. Service, R. F. Liquid Sunshine. *Science (80-.).* **361**, 120–123 (2018).

172. Christensen, C. H., Johannessen, T., Sørensen, R. Z. & Nørskov, J. K. Towards an ammonia-mediated hydrogen economy? *Catal. Today* **111**, 140–144 (2006).

173. Soloveichik, G. ARPA-E REFUEL Program: Distributed Production of Ammonia and its Conversion to Energy. in *2019 AIChE Annual Meeting* (AIChE, 2019).

174. Kerru, N., Gummidi, L., Maddila, S., Gangu, K. K. & Jonnalagadda, S. B. A Review on Recent Advances in Nitrogen-Containing Molecules and Their Biological Applications. *Molecules* **25**, 1909 (2020).

175. Chen, C. *et al.* Coupling N2 and CO2 in H2O to synthesize urea under ambient conditions. *Nat. Chem.* **12**, 717–724 (2020).

176. Nielander, A. C. *et al.* Readily Constructed Glass Piston Pump for Gas Recirculation. *ACS Omega*

5, 16455–16459 (2020).

177. Tang, C. & Qiao, S.-Z. How to explore ambient electrocatalytic nitrogen reduction reliably and insightfully. *Chem. Soc. Rev.* **48**, 3166–3180 (2019).

178. Kang, C. S. M., Zhang, X. & MacFarlane, D. R. High Nitrogen Gas Solubility and Physicochemical Properties of [C 4 mpyr][eFAP]–Fluorinated Solvent Mixtures. *J. Phys. Chem. C* **123**, 21376–21385 (2019).

179. Shi, R., Zhang, X., Waterhouse, G. I. N., Zhao, Y. & Zhang, T. The Journey toward Low Temperature, Low Pressure Catalytic Nitrogen Fixation. *Adv. Energy Mater.* **10**, (2020).

180. Munter, T. R., Bligaard, T., Christensen, C. H. & Nørskov, J. K. BEP relations for N2 dissociation over stepped transition metal and alloy surfaces. *Phys. Chem. Chem. Phys.* **10**, 5202 (2008).

181. Yu, W. *et al.* Cathodic NH 4 + leaching of nitrogen impurities in CoMo thin-film electrodes in aqueous acidic solutions. *Sustain. Energy Fuels* **4**, 5080–5087 (2020).

182. Chen, Y. *et al.* Revealing nitrogen-containing species in commercial catalysts used for ammonia electrosynthesis. *Nat. Catal.* **3**, (2020).

This paper shows that various commercially sold pure metals contain significant N-containing contamination, and provides a way to measure these contaminants.

183. Hargreaves, J. S. J. Heterogeneous catalysis with metal nitrides. *Coord. Chem. Rev.* **257**, 2015–2031 (2013).

184. Krauth, O., Fahsold, G. & Lehmann, A. Surface-enhanced infrared absorption. *Surf. Sci.* **433**, 79–82 (1999).

185. Yao, Y., Zhu, S., Wang, H., Li, H. & Shao, M. A Spectroscopic Study on the Nitrogen Electrochemical Reduction Reaction on Gold and Platinum Surfaces. *J. Am. Chem. Soc.* **140**, 1496–1501 (2018).

186. Yao, Y., Wang, H., Yuan, X. Z., Li, H. & Shao, M. Electrochemical Nitrogen Reduction Reaction on Ruthenium. *ACS Energy Lett.* **4**, 1336–1341 (2019).

187. Matsui, T. *et al.* In Situ Attenuated Total Reflection Infrared Spectroscopy on Electrochemical Ammonia Oxidation over Pt Electrode in Alkaline Aqueous Solutions. *Langmuir* **31**, 11717–11723 (2015).

188. Abdiaziz, K., Salvadori, E., Sokol, K. P., Reisner, E. & Roessler, M. M. Protein film electrochemical EPR spectroscopy as a technique to investigate redox reactions in biomolecules. *Chem. Commun.* **55**, 8840–8843 (2019).

189. Bajada, M. A. *et al.* A Precious-Metal-Free Hybrid Electrolyzer for Alcohol Oxidation Coupled to CO2-to-Syngas Conversion. *Angew. Chemie Int. Ed.* **59**, 15633–15641 (2020).

190. Joris, G. G. & Taylor, H. S. Exchange reactions of nitrogen isotopes on iron and tungsten surfaces. *J. Chem. Phys.* **7**, 893–898 (1939).

191. Urabe, K. Activation of nitrogen by alkali metal-promoted transition metal II. Isotopic exchange in molecular nitrogen over potassium-promoted ruthenium-carbon catalyst. *J. Catal.* **32**, 108–113 (1974).

192. Urabe, K. Activation of nitrogen by alkali metal-promoted transition metal VI. Hydrogen effect on isotopic equilibration of nitrogen and rate-determining step of ammonia synthesis on potassium-promoted ruthenium catalysts. *J. Catal.* **42**, 197–204 (1976).

193. Hunter, S. M. *et al.* A study of 15N/14N isotopic exchange over cobalt molybdenum nitrides. *ACS Catal.* **3**, 1719–1725 (2013).

194. Hargreaves, J. S. J. Nitrides as ammonia synthesis catalysts and as potential nitrogen transfer reagents. *Appl. Petrochemical Res.* (2014).

195. Shannon, S. L. & Goodwin, J. G. Characterization of Catalytic Surfaces by Isotopic-Transient Kinetics during Steady-State Reaction. *Chem. Rev.* **95**, 677–695 (1995).

196. Nwalor, J. Steady-state isotopic transient-kinetic analysis of iron-catalyzed ammonia synthesis. *J. Catal.* **117**, 121–134 (1989).

197. Nwalor, J. U. & Goodwin, J. G. Isotopic tracing study of K promotion of NH3 synthesis on Ru. *Top. Catal.* **1**, 285–293 (1994).

198. McClaine, B. Isotopic Transient Kinetic Analysis of Cs-Promoted Ru/MgO during Ammonia Synthesis. *J. Catal.* **210**, 387–396 (2002).

199. McClaine, B. C. & Davis, R. J. Importance of Product Readsorption during Isotopic Transient Analysis of Ammonia Synthesis on Ba-Promoted Ru/BaX Catalyst. *J. Catal.* **211**, 379–386 (2002).

200. Siporin, S. Isotopic transient analysis of ammonia synthesis over Ru/MgO catalysts promoted by cesium, barium, or lanthanum. *J. Catal.* **222**, 315–322 (2004).

201. Schlesinger, W. & Hartley, A. A global budget for atmospheric NH3. *Biogeochemistry* **15**, 191–211 (1992).

202. Vojvodic, A. *et al.* Exploring the limits: A low-pressure, low-temperature Haber-Bosch process. *Chem. Phys. Lett.* (2014).

203. Spinelli, J. B., Kelley, L. P. & Haigis, M. C. An LC-MS Approach to Quantitative Measurement of Ammonia Isotopologues. *Sci. Rep.* **7**, 10304 (2017).

204. Liu, Y. *et al.* Facile All-Optical Method for In Situ Detection of Low Amounts of Ammonia. *iScience* **23**, 101757 (2020).

205. Mou, S., Wang, H. & Sun, Q. Simultaneous determination of the three main inorganic forms of nitrogen by ion chromatography. *J. Chromatogr. A* **640**, 161–165 (1993).

206. Andersen, S. Z. Electrochemical Nitrogen Reduction Under (Near) Ambient Conditions. *Technical University of Denmark* (2020).

207. Timmer, B. H., van Delft, K. M., Otjes, R. P., Olthuis, W. & van den Berg, A. Miniaturized measurement system for ammonia in air. *Anal. Chim. Acta* **507**, 137–143 (2004).

208. Kim, K., Yoo, C.-Y., Kim, J.-N., Yoon, H. C. & Han, J.-I. Electrochemical Synthesis of Ammonia from Water and Nitrogen in Ethylenediamine under Ambient Temperature and Pressure. *J. Electrochem. Soc.* **163**, F1523–F1526 (2016).

209. Sato, K. *et al.* A low-crystalline ruthenium nano-layer supported on praseodymium oxide as an active catalyst for ammonia synthesis. *Chem. Sci.* **8**, 674–679 (2017).

210. Chang, F. *et al.* Alkali and Alkaline Earth Hydrides-Driven N2 Activation and Transformation over Mn Nitride Catalyst. *J. Am. Chem. Soc.* **140**, 14799–14806 (2018).

211. Kitano, M. *et al.* Low-Temperature Synthesis of Perovskite Oxynitride-Hydrides as Ammonia Synthesis Catalysts. *J. Am. Chem. Soc.* **141**, 20344–20353 (2019).

212. Kitano, M. *et al.* Self-organized Ruthenium-Barium Core-Shell Nanoparticles on a Mesoporous Calcium Amide Matrix for Efficient Low-Temperature Ammonia Synthesis. *Angew. Chemie Int. Ed.* **57**, 2648–2652 (2018).

213. Wang, Y. *et al.* Generating Defect-Rich Bismuth for Enhancing the Rate of Nitrogen Electroreduction to Ammonia. *Angew. Chemie Int. Ed.* **58**, 9464–9469 (2019).

214. Kong, J. *et al.* Electrochemical Synthesis of NH 3 at Low Temperature and Atmospheric Pressure Using a γ-Fe 2 O 3 Catalyst. *ACS Sustain. Chem. Eng.* **5**, 10986–10995 (2017).

215. Shi, M.-M. *et al.* Au Sub-Nanoclusters on TiO2 toward Highly Efficient and Selective Electrocatalyst for N2 Conversion to NH3 at Ambient Conditions. *Adv. Mater.* **29**, 1606550 (2017).

216. Zhang, N. *et al.* Refining Defect States in W18O49 by Mo Doping: A Strategy for Tuning N 2 Activation towards Solar-Driven Nitrogen Fixation. *J. Am. Chem. Soc.* **140**, 9434–9443 (2018).

217. Wang, S. *et al.* Light-Switchable Oxygen Vacancies in Ultrafine Bi5O7Br Nanotubes for Boosting Solar-Driven Nitrogen Fixation in Pure Water. *Adv. Mater.* **29**, 1701774 (2017).

218. Jang, Y. J., Lindberg, A. E., Lumley, M. A. & Choi, K. S. Photoelectrochemical Nitrogen Reduction to Ammonia on Cupric and Cuprous Oxide Photocathodes. *ACS Energy Lett.* **5**, 1834–1839 (2020).

219. Zhu, D., Zhang, L., Ruther, R. E. & Hamers, R. J. Photo-illuminated diamond as a solid-state source of solvated electrons in water for nitrogen reduction. *Nat. Mater.* **12**, 836–841 (2013).

220. Wang, X. *et al.* Insight into dynamic and steady-state active sites for nitrogen activation to ammonia by cobalt-based catalyst. *Nat Commun* **11**, 653 (2020).

221. Ogura, Y. *et al.* Efficient ammonia synthesis over a Ru/La 0.5 Ce 0.5 O 1.75 catalyst pre-reduced at high temperature. *Chem. Sci.* **9**, 2230–2237 (2018).

222. Hodgetts, R. Y. *et al.* Refining Universal Procedures for Ammonium Quantification via Rapid 1 H NMR Analysis for Dinitrogen Reduction Studies. *ACS Energy Lett.* **5**, 736–741 (2020).

This paper assesses the sensitivity of nuclear magnetic resonance towards the detection of ammonia in solutions with different proton concentration

Glossary Terms

Faradaic Efficiency: The efficiency at which charge, in the form of electrons, participate in a specific electrochemical reaction

Activation barriers: The minimal amount of energy required for reactants to undergo a chemical reaction This is the energy difference between the reactant and the transition state.

Standard potential: The potential (V) of a reversible electrode at standard state with ions at an effective 1 M concentration at the pressure of 1 atm.

Electrochemical half-cell reactions: Either an oxidation reaction on the anode electrode where an electron is lost or a reduction reaction on the cathode electrode where an electron is gained.

Electric arc-generated hot plasma: A discharge of electric current across a spatial gap, sustained by the presence of a thermally ionized plasma, which allows for the flow of said current.

Reaction orders: the power dependence of the rate on the concentration of each reactant, which is an experimentally determined parameter that can have fraction values.

Tafel analysis: is used to determine an electrochemical systems transfer coefficient via voltammograms, thereby providing information about the electrochemical mechanism and catalytic activity.

Ohmic correction: Accounting for the Ohmic resistance of the media to accurately determine the potential at the surface of the electrode.

Quantum yield: Determining the number of times a specific event occurs per absorbed photon by the system in question.

Density functional theory: a computational quantum mechanical modelling method used to investigate the electronic structure of many-body systems.

Zero point energy: The lowest possible energy that a quantum mechanical system contains, which includes fluctuations in the lowest energy state from the Heisenberg uncertainty principle.

Pareto-optimal frontier: A curve which contains physically possible optimal trade-offs between activity and stability

Physisorption: Also called physical adsorption, is a weak intermolecular attraction via van der Waals forces, which results in the development of monolayers or multilayers of adsorbates upon a surface.

RAT

Nature Reviews Methods Primers thanks ref name, ref name and the other, anonymous, reviewer(s) for their contribution to the peer review of this work.

TOC blurb

This Primer highlights the range of new strategies for sustainable N_2 activation and the step-by-step protocol necessary for evaluating genuine activity. The required metrics and how to interpret data alongside the best practices to improve reproducibility and enable the development of practical technologies are discussed.